

1 July 17, 2016

2

3 Dear Editor,

4

5 We appreciate the reviewers' suggestions which have considerably improved the manuscript
6 (**acp-2015-939**). Enclosed are point-by-point responses to the reviewers. We hope that with
7 these changes the manuscript will be suitable for publication in "**Atmospheric Chemistry**
8 **and Physics**"

9

10 Thank you very much.

11 Sincerely,

12 Seung-Muk Yi

13

14 Professor, Dept. of Environmental Health, Graduate School of Public Health
15 Seoul National University, 1 Gwanak-ro, Gwanak-gu, Seoul 151-742, South Korea
16 Telephone: (82) 2-880-2736, Fax: (82) 2-762-9105, E-mail: yiseung@snu.ac.kr

17

18 **Response to Anonymous Referees' Comments**

19

20 • Journal: ACP

21 • Title: Characteristics of total gaseous mercury (TGM) concentrations in an industrial

22 complex in southern Korea: Impacts from local sources

23 • Author(s): Yong-Seok Seo, Seung-Pyo Jeong, Thomas M. Holsen, Young-Ji Han, Eunhwa Choi,

24 Eun Ha Park, Tae Young Kim, Hee-Sang Eum, Dae Gun Park, Eunhye Kim, Soontae Kim, Jeong-

25 Hun Kim, Jaewon Choi, Seung-Muk Yi

26 • MS No.: acp-2015-939

27 • MS Type: Research article

28 • Status: File Upload (ACP)

29 • Iteration: Minor Revision

30 • Special Issue: Data collection, analysis and application of speciated atmospheric mercury

31

32 **Response to Anonymous Referee #1:**

33

34 **Comment 1**

35 Line 195: “The extension to the bivariate case can provide more information on the nature of
36 the sources because different source types such as stack emission sources and ground-level
37 sources can have different wind speed dependencies (prominent at low and high wind speed).”
38 This statement is incorrect because wind speeds are higher at higher elevation than at ground
39 level. It also contradicts a related sentence in lines 439-456: “CBPF shows that the high
40 probabilities from the west occurred under high wind speed (>3 m s⁻¹) indicative of emissions
41 from stacks as well as low wind speed (≤ 3 m s⁻¹) indicative of non-buoyant ground level
42 sources”

43

44 **Response 1**

45 The reviewer is correct – we reversed the order in this sentence. The corrected version is
46 shown below (Please see the [Line 225-228](#)).

47

48 *“The extension to the bivariate case can provide more information on the nature of the sources
49 because different source types such as stack emission sources and ground-level sources can
50 have different wind speed dependencies (**prominent at high and low wind speed, respectively**).”*

51

52

53 **Comment 2**

54 Section 5.1: This paragraph seems out of place. The wind direction analysis should be
55 integrated with the mercury results rather than having its own section. The major result is the
56 mercury analysis rather than the wind direction analysis.

57

58 **Response 2**

59 This section is meant to provide background and context for the Hg results. To improve the
60 presentation we have moved this paragraph to section 2.2 and labeled it: “Meteorological
61 Setting” as shown below (Please see the [Line 180-184](#)):

62

63 *2.2. Meteorological data*

64 *Hourly meteorological data (air temperature, relative humidity, and wind speed and direction)*

65 were obtained from the Automatic Weather Station (AWS) operated by the Korea
66 Meteorological Administration (KMA) (<http://www.kma.go.kr>) (6 km from the site). Hourly
67 concentrations of NO_2 , O_3 , CO , PM_{10} and SO_2 were obtained from the National Air Quality
68 Monitoring Network (NAQMN) (3 km from the site) (Fig. 1).

69 Meteorological Setting. Fig. S1 shows the frequency of counts of measured wind direction
70 occurrence by season during the sampling period. The predominant wind direction at the
71 sampling site was W (20.9%) and WS (19.2%), and calm conditions of wind speed less than 1
72 $m s^{-1}$ occurred 7.6% of the time. Compared to other seasons, however, the prevailing winds in
73 summer were N (17.0%), NE (16.4%), S (16.4%), and SW (15.8%).

74

75

76 **Comment 3**

77 Line 293-294: “however considerably lower than those measured near large Hg sources in
78 Guangzhou, China (Table 1).” This is compared to a much older study. TGM in Guangzhou
79 from a more recent study in Table 1 was 4.6 ng/m³, which is similar to the average TGM in
80 this study.

81

82 **Response 3**

83 Thank you for this updated reference. We corrected **Table 1** on **Line 561** and rephrased the
84 sentence as follows on **Line 316-317**.

85

86 “*...and those measured in China, in Japan and other locations in Korea, however lower than*
87 *those measured at Changchun, Gui Yang and Nanjing in China (Table 1).*”

88

89

90 **Comment 4**

91 Section 5.5 diurnal variations: The higher daytime than nighttime result is not quite correct. As
92 stated in lines 365-366, “TGM generally showed a consistent diurnal variation with an increase
93 in the early morning (06:00-09:00) and a decrease in the afternoon (14:00-17:00).” The daytime
94 period from 6:00-18:00 includes the morning increase and afternoon decrease; therefore it’s
95 unclear if daytime TGM is really higher. I suggest explaining what caused the early morning
96 increase and afternoon decrease in TGM, instead of the cause for higher daytime TGM in
97 general. There were a few instances where it led to confusing results. E.g. line 384, “the higher

98 concentrations in the daytime than those in nighttime were due to local emission sources
99 because the daytime temperature ($14.7 \pm 10.0^{\circ}\text{C}$) was statistically significantly higher than that
100 in the nighttime ($13.0 \pm 9.8^{\circ}\text{C}$) (t-test, $p < 0.05$) and there was a weak but statistically
101 significant negative correlation between TGM concentration and ambient air temperature ($r =$
102 -0.08) ($p < 0.05$). The negative correlation between TGM and temperature is inconsistent with
103 the higher daytime TGM. Another example in line 406, “TGM concentration was negatively
104 correlated with ambient air temperature ($r = -0.08$) ($p < 0.05$) because high ambient air
105 temperature in the daytime will increase the height of the boundary layer and dilute the TGM,
106 and the relatively lower boundary layer at nighttime could concentrate the TGM in the
107 atmosphere (Li et al., 2011).” This explanation contradicts higher daytime TGM as well. It only
108 explains why TGM is lower in the afternoon, but not the early morning increase.
109

110 **Response 4**

111 To clarify this section the day-night concentration variation and morning-afternoon variation
112 during the day were discussed separately as shown below. Please see the Section 5.4 on [Line](#)
113 [384-458](#).

114
115 “*Diurnal variations of TGM (Fig. 3), co-pollutants concentrations, and meteorological*
116 *data were observed (Fig. S4). TGM, O₃, CO, SO₂, and temperature in the daytime (06:00-*
117 *18:00) were higher than those in the nighttime (18:00-06:00) ($p < 0.05$) except PM₁₀ ($p =$
118 0.09) (Fig. S5). However, NO₂ during the nighttime because of relatively lower*
119 *photochemical reactivity with O₃ was higher than that in daytime ($p < 0.05$) (Adame et al.,*
120 *2012).*

121 *The daytime TGM concentration ($5.3 \pm 4.7 \text{ ng m}^{-3}$) was higher than that in the nighttime*
122 *($4.7 \pm 4.7 \text{ ng m}^{-3}$) ($p < 0.01$), which was similar to several previous studies (Cheng et al.,*
123 *2014; Gabriel et al., 2005; Nakagawa, 1995; Stamenkovic et al., 2007) but different than*
124 *another studies (Lee et al., 1998). Previous studies reported that this different is due to local*
125 *sources close to the sampling site (Cheng et al., 2014; Gabriel et al., 2005), a positive*
126 *correlation between TGM concentration and ambient air temperature (Nakagawa, 1995) and*
127 *increased traffic (Stamenkovic et al., 2007). However, another study suggested that the*
128 *higher TGM concentration during the night was due to the shallowing of the boundary layer,*
129 *which concentrated the TGM near the surface (Lee et al., 1998).*

130 In a previous study the daytime TGM concentration was relatively lower than that in the
131 nighttime because the sea breeze transported air containing low amounts of TGM from the
132 ocean during the daytime whereas the land breeze transported air containing relatively high
133 concentrations of TGM from an urban area during the nighttime (Kellerhals et al., 2003).
134 Although it is possible that the land-sea breeze may affect diurnal variations in TGM
135 concentrations since the sampling site was near the ocean and lower TGM were also
136 observed during the daytime, the higher concentrations in the daytime than those in nighttime
137 were due to local emission sources because the daytime temperature (14.7 ± 10.0 °C) was
138 statistically significantly higher than that in the nighttime (13.0 ± 9.8 °C) (*t*-test, $p < 0.05$)
139 and there was a weak but statistically significant negative correlation between TGM
140 concentration and ambient air temperature ($r = -0.08$) ($p < 0.05$). In addition, there are
141 several known Hg sources such as iron and steel manufacturing facilities including electric
142 and sintering furnaces using coking between the sampling site and the ocean.

143 As shown in *Fig. 3* and *Fig. S4*, there was a weak but negative relationship between the
144 TGM concentrations and O_3 concentrations ($r = -0.18$) ($p < 0.01$), suggesting that oxidation
145 of GEM in the oxidizing atmosphere during periods of strong atmospheric mixing was
146 partially responsible for the diurnal variations of TGM concentrations. In addition, oxidation
147 of GEM by bromine species in the coastal area (Obrist et al., 2011) or by chloride radicals in
148 marine boundary layer (Laurier et al., 2003) might play a significant role. If oxidation of
149 GEM occurred, GOM concentrations would increase. However there are uncertainties on the
150 net effects on TGM (the sum of the GEM and the GOM) since we did not measure GOM
151 concentrations.

152 TGM concentration was negatively correlated with ambient air temperature ($r = -0.08$)
153 ($p < 0.05$) because high ambient air temperature in the daytime will increase the height of
154 the boundary layer and dilute the TGM, and the relatively lower boundary layer at nighttime
155 could concentrate the TGM in the atmosphere (Li et al., 2011). Although there was a
156 statistically significant negative correlation between the TGM concentration and ambient air
157 temperature, there was a rapid increase in TGM concentration between 06:00-09:00 when
158 ambient temperatures also increased possibly due to local emissions related to industrial
159 activities, increased traffic, and activation of local surface emission sources. Similar patterns
160 were found in previous studies (Li et al., 2011; Stamenkovic et al., 2007). Nonparametric
161 correlations revealed that there is a weak positive correlation between TGM and ambient air
162 temperature ($r_s = 0.11$, $p=0.27$) between 06:00-09:00. The TGM concentration was

163 *negatively correlated with O₃ ($r_s = -0.33$, $p < 0.01$) but positively correlated with NO₂ ($r_s =$
164 0.21 , $p < 0.05$), suggesting that the increased traffic is the main source of TGM during these
165 time periods.*

166 *Compared to other seasons, significantly different diurnal variations of TGM were
167 observed in fall. The daytime TGM concentrations in fall were similar to those in other
168 seasons, however, the nighttime TGM concentrations in fall were much higher than other
169 seasons. As described earlier in Section 5.2, the high TGM concentrations in fall was
170 possibly due to the relationship between other pollutants and meteorological conditions as
171 well as different wind direction and sources. The nighttime TGM concentrations in fall were
172 simultaneously positively correlated with PM₁₀ ($r=0.26$) ($p < 0.05$) and CO ($r=0.21$) ($p < 0.05$)
173 concentrations and wind speed ($r=0.35$) ($p < 0.01$), suggesting that the combustion process is
174 an important source during this period.*

175 *TGM generally showed a consistent increase in the early morning (06:00-09:00) and a
176 decrease in the afternoon (14:00-17:00), similar to previous studies (Dommergue et al.,
177 2002; Friedli et al., 2011; Li et al., 2011; Liu et al., 2011; Mao et al., 2008; Shon et al.,
178 2005; Song et al., 2009; Stamenkovic et al., 2007). Significantly different diurnal patterns
179 have been observed at many suburban sites with the daily maximum occurring in the
180 afternoon (12:00-15:00), possibly due to local emission sources and transport (Fu et al.,
181 2010; Fu et al., 2008; Kuo et al., 2006; Wan et al., 2009). Other studies in Europe reported
182 that TGM concentrations were relatively higher early in the morning or at night possibly due
183 to mercury emissions from surface sources that accumulated in the nocturnal inversion layer
184 (Lee et al., 1998; Schmolke et al., 1999).*

185 *Based on the above results, the diurnal variations in TGM concentration are due to a
186 combination of: 1) reactions with an oxidizing atmosphere, 2) changes in ambient temperature
187 and 3) local emissions related to industrial activities. To supplement these conclusions CPF
188 and CBPF were used to identify source directions and TPSCF was used to identify potential
189 source locations.”*

190

191

192 **Comment 5**

193 Section 5.6 line 448: “It is difficult to discuss about the different seasonal patterns for CPF and
194 CBPF for TGM concentrations since there were no correlations between TGM and other
195 pollutants in spring, summer and fall except O3.” I don’t understand (and not mentioned in the

196 paper) why the correlation results are needed to interpret the seasonal patterns of CPF and
197 CBPF (Fig. S6). It wasn't needed to explain the overall CPF and CBPF results. Also, I'm still
198 skeptical whether CBPF provides more information about sources than CPF. Wind speed
199 dependency is included in CBPF to differentiate between ground level and stack emissions;
200 however, it's not discussed in the results. There should be a more detailed discussion of the
201 local ground level and stack emissions and uncertainties and disadvantages with the CBPF
202 method.

203

204 **Response 5**

205 In order to clarify, we have deleted the following sentence.

206

207 *“It is difficult to discuss about the different seasonal patterns for CPF and CBPF for TGM
208 concentrations since there were no correlations between TGM and other pollutants in spring,
209 summer and fall except O₃. ”*

210

211 **Response to Anonymous Referee #2:**

212

213 **Comment 1**

214 Section 2 through 5 and conclusion are well improved. However, introduction section needs
215 more work. Please re-organize and add recent literature reviews that are related with this
216 research. Each paragraph contains one topic sentence. Please look at the introduction section.
217 What is the topic sentence for each paragraph?

218 **Response 1**

219 Thank you for your comments. As suggested, we carefully revised and edited including adding
220 recent literature reviews that are related with this research as follows on **Line 71-80, Line 91-**
221 **95, Line 109, Line 118-133** as shown below..

222

223 *“Mercury (Hg) is an environmental toxic and bioaccumulative trace metal whose
224 emissions to the environment have considerably increased due to anthropogenic activities
225 such as mining and combustion processes (Pirrone et al., 2013; Streets et al., 2011). Hg can
226 be globally distributed from the sources through atmospheric transport as gaseous elemental
227 form (Bullock et al., 1998; Mason and Sheu, 2002). However, the origins of atmospheric
228 mercury are local and regional (Choi et al., 2009) as well as hemispherical and global
229 (Durnford et al., 2010). In addition to the general background concentration of Hg in the
230 global atmosphere, local Hg emissions contribute to the Hg burden and it contribute to the
231 background concentration much of which represents anthropogenic releases accumulated
232 over the decades (UNEP, 2002).*

233 *Hg in the atmosphere exists in three major inorganic forms including gaseous elemental
234 mercury (GEM, Hg^0), gaseous oxidized mercury (GOM, Hg^{2+}) and particulate bound
235 mercury (PBM, $Hg(p)$). GEM which is the dominant form of Hg in ambient air, (>95%) has a
236 relatively long residence time (0.5~2 years) due to its low reactivity and solubility (Schroeder
237 and Munthe, 1998). However, GOM has high water solubility and relatively strong surface
238 adhesion properties (Han et al., 2005), so it has a short atmospheric residence time (~days).
239 PBM is associated with airborne particles such as dust, soot, sea-salt aerosols, and ice
240 crystals (Lu and Schroeder, 2004) and is likely produced, in part, by adsorption of GOM
241 species such as $HgCl_2$ onto atmospheric particles (Gauchard et al., 2005; Lu and Schroeder,
242 2004; Sakata and Marumoto, 2005; Seo et al., 2015).*

243 Atmospheric Hg released from natural (e.g., volcanoes, volatilization from aquatic and
244 terrestrial environments) (Pirrone et al., 2010; Strode et al., 2007) and anthropogenic
245 sources (e.g., coal combustion, cement production, ferrous and non-ferrous metals
246 manufacturing facilities, waste incineration and industrial boilers) (Pacyna et al., 2010;
247 Pacyna et al., 2006; Pacyna et al., 2003; Pirrone et al., 2010; Zhang et al., 2015) when
248 introduced into terrestrial and aquatic ecosystem through wet and dry deposition (Mason and
249 Sheu, 2002) can undergo various physical and chemical transformations before being
250 deposited. Its lifetime in the atmosphere depends on its reactivity and solubility so that,
251 depending on its form, it can have impacts on local, regional and global scales (Lin and
252 Pehkonen, 1999; Lindberg et al., 2007). A portion of the Hg deposited in terrestrial
253 environments through direct industrial discharge or atmospheric deposition is transported to
254 aquatic system through groundwater and surface water runoff (Miller et al., 2013). A
255 previous study also reported that Hg directly released into terrestrial and aquatic ecosystems
256 from industrial effluent has influenced surface water, sediment and biological tissue
257 (Flanders et al., 2010). Significant spatial variations in atmospheric Hg deposition near
258 urban and industrial areas are due to local anthropogenic sources including municipal waste
259 incinerators, medical waste incinerators, electric power generating facilities and cement
260 kilns (Dvonch et al., 1998), ferrous and non-ferrous metal processing, iron and steel
261 manufacturing facilities, oil and coal combustion (Hoyer et al., 1995), and other forms of
262 industrial combustion (Brown et al., 2015). Miller et al. (2013) also reported that local
263 sources of elemental Hg are typically industrial processes including retort facilities used in
264 the mercury mining industry to convert Hg containing minerals to elemental Hg and chlor-
265 alkali facilities.

266 The annual average national anthropogenic Hg emissions from South Korea in 2007 have
267 been estimated to be 12.8 tons (range 6.5 to 20.2 tons); the major emission sources are coal
268 combustion in thermal power plants (25.8%), oil refineries (25.5%), cement kilns (21%),
269 incinerators (19.3%) including sludge incinerators (4.7%), municipal waste incinerators
270 (MWIs) (3%), industrial waste incinerators (IWIs) (2.7%), hospital/medical/infectious waste
271 incinerators (HMIWIs) (8.8%), and iron manufacturing (7%) (Kim et al., 2010). Global
272 anthropogenic Hg emissions were estimated to be 1960 tons in 2010 with East and Southeast
273 Asia responsible for 777 tons (39.7%) (19.6 tons for Japan and 8.0 tons for South Korea)
274 (AMAP/UNEP, 2013). China is the largest Hg emitting country in the world, contributing

275 more than 800 tons (~ 40%) of the total anthropogenic Hg emissions (UNEP, 2008).

276 *Background atmospheric Hg concentrations in the northern hemisphere have decreased*
277 *since 1996 (Slemr et al., 2003), as measured at the Global Atmosphere Watch (GAW) station*
278 *at Mace Head, Ireland (Ebinghaus et al., 2011) and at the Canadian Atmospheric Mercury*
279 *Network (CAMNet) (Temme et al., 2007). In urban areas in South Korea atmospheric TGM*
280 *concentrations have also decreased over the last few decades due to the reduced fossil fuel*
281 *(mainly anthracite coal) consumption (Kim et al., 2016; Kim and Kim, 2000). However, this*
282 *decreasing trend is inconsistent with steady or increasing global anthropogenic Hg emissions*
283 *since 1990 in the northern hemisphere (Streets et al., 2011; Weigelt et al., 2015; Wilson et al.,*
284 *2010). A previous study reported that the global anthropogenic Hg emissions are increasing*
285 *with an average of 1.3% annual growth without including the artisanal and small-scale*
286 *production sector (Muntean et al., 2014).*

287 *Receptor models are often used to identify sources of air pollutants and are focused on*
288 *the pollutants behavior in the ambient environment at the point of impact (Hopke, 2003). In*
289 *previous studies, conditional probability function (CPF), which utilizes the local wind*
290 *direction, and potential source contribution function (PSCF), which utilizes longer backward*
291 *trajectories (typically 3-5 days), combined with concentration data were used to identify*
292 *possible transport pathways and source locations (Hopke, 2003). While PSCF has been used*
293 *primarily to identify regional sources, it has also been used to identify local sources (Hsu et*
294 *al., 2003).*

295 *The objectives of this study were to characterize the hourly and seasonal variations of*
296 *atmospheric TGM (the sum of the GEM and the GOM) concentrations, to identify the*
297 *relationships between TGM and co-pollutant concentrations, and to identify likely source*
298 *directions and locations of TGM using CPF, conditional bivariate probability function*
299 *(CBPF) and total PSCF (TPSCF)."*

300

301

302 **Comment 2**

303 The 2nd paragraph (line 81-84) could be moved.

304 **Response 2**

305 We have deleted the paragraph (Line 81-84) and combined with next paragraph as follows on

306 **Line 91-95.**
307
308 “Atmospheric Hg released from natural (e.g., volcanoes, volatilization from aquatic and
309 terrestrial environments) (Pirrone et al., 2010; Strode et al., 2007) and anthropogenic sources
310 (e.g., coal combustion, cement production, ferrous and non-ferrous metals manufacturing
311 facilities, waste incineration and industrial boilers) (Pacyna et al., 2010; Pacyna et al., 2006;
312 Pacyna et al., 2003; Pirrone et al., 2010; Zhang et al., 2015) when introduced into...”

313
314

315 **Comment 3**

316 The 3rd (line 85-92), the 4th (line 93-95), and 5th (line 96-103) paragraphs have same topics
317 so they could be combined into one.

318 **Response 3**

319 As suggested, the sentences were combined into one paragraph on **Line 91-112**.

320
321

322 **Comment 4**

323 In the 6th paragraph (line 104-109), the author talked about the Hg emissions in South Korea.
324 Is this urban areas or both urban and rural areas? Which year? How about other counties near
325 South Korea? (e.g., China, Japan?)

326 **Response 4**

327 Kim et al. (2010) reported that the annual average national (including urban and rural areas)
328 anthropogenic Hg emissions from South Korea in 2007 have been estimated to be 12.8
329 tons ranged from 6.5 to 20.2 tons.

330
331

332 In response to this comment, we have rephrased the sentence as follows on **Line 113-114**.

333
334

335 “*The annual average national anthropogenic Hg emissions from South Korea in 2007 have*
336 *been estimated to be 12.8 tons (range 6.5 to 20.2 tons);*”

337
338

339 We added the sentence about Hg emissions from China and Japan as follows on **Line 118-122**.

339 *Southeast Asia responsible for 777 tons (39.7%) (19.6 tons for Japan and 8.0 tons for South*
340 *Korea) (AMAP/UNEP, 2013). China is the largest Hg emitting country in the world,*
341 *contributing more than 800 tons (~ 40%) of the total anthropogenic Hg emissions (UNEP,*
342 *2008)."*

343

344

345 **Comment 5**

346 Line 117-121: should be one paragraph

347 **Response 5**

348 As suggested, we separated two paragraphs as follows on **Line 142-146**.

349

350 *".... While PSCF has been used primarily to identify regional sources, it has also been used to*
351 *identify local sources (Hsu et al., 2003).*

352 *The objectives of this study were to characterize the hourly and seasonal variations of*
353 *atmospheric TGM (the sum of the GEM and the GOM) concentrations, to identify the*
354 *relationships between TGM and co-pollutant concentrations, and to identify likely source*
355 *directions and locations of TGM using CPF, conditional bivariate probability function (CBPF)*
356 *and total PSCF (TPSCF).*"

357

1 **Characteristics of total gaseous mercury (TGM) concentrations in an
2 industrial complex in southern Korea: Impacts from local sources**

4 Yong-Seok Seo^{1, 2}, Seung-Pyo Jeong¹, Thomas M. Holsen³, Young-Ji Han⁴, Eun
5 Ha Park¹, Tae Young Kim¹, Hee-Sang Eum¹, Dae Gun Park¹, Eunhye Kim⁶, Soontae Kim⁶,
6 Jeong-Hun Kim⁷, Jaewon Choi⁸, Seung-Muk Yi^{1, 2, *}

8 ¹Department of Environmental Health, Graduate School of Public Health, Seoul National
9 University, 1 Gwanak, Gwanak-ro, Gwanak-gu, Seoul 151-742, South Korea

11 ²Institute of Health and Environment, Seoul National University, 1 Gwanak, Gwanak-ro,
12 Gwanak-gu, Seoul 151-742, South Korea

14 ³Department of Civil and Environmental Engineering, Clarkson University, Potsdam,
15 NY13699, USA

17 ⁴Department of Environmental Science, Kangwon National University, 192-1, Hyoja-2-dong,
18 Chuncheon, Kangwondo, 200-701, South Korea

20 ⁵Asian Institute for Energy, Environment & Sustainability, Seoul National University, 1
21 Gwanak-ro, Gwanak-gu, Seoul 151-742, South Korea

23 ⁶Department of Environmental, Civil and Transportation Engineering, Ajou University,
24 Woncheon-dong, Yeongtong-gu, Suwon, 443-749, South Korea

26 ⁷Division of Air Pollution Engineering, Department of Climate and Air Quality Research,
27 National Institute of Environmental Research, Hwangyong-ro 42, Seogu, Incheon, 404-708,
28 South Korea

30 ⁸University of Pennsylvania, Philadelphia, PA19104, USA

40 *Address correspondence to Dr. Seung-Muk Yi, Graduate School of Public Health, Seoul
41 National University, 1 Gwanak, Gwanak-ro, Gwanak-gu, Seoul 151-742, South Korea
42 E-mail) yiseung@snu.ac.kr
43 Telephone) 82-2-880-2736
44 Fax) 82-2-745-9104

45 **Abstract**

46 Total gaseous mercury (TGM) concentrations were measured every 5 min in Pohang,
47 Gyeongsangbuk-do, Korea during summer (17 August~23 August 2012), fall (9 October~17
48 October 2012), winter (22 January ~29 January 2013), and spring (26 March~3 April 2013)
49 to: 1) characterize the hourly and seasonal variations of atmospheric TGM concentrations, 2)
50 identify the relationships between TGM and co-pollutants, and 3) identify likely source
51 directions and locations of TGM using conditional probability function (CPF), conditional
52 bivariate probability function (CBPF) and total potential source contribution function
53 (TPSCF).

54 The TGM concentration was statistically significantly highest in fall ($6.7 \pm 6.4 \text{ ng m}^{-3}$),
55 followed by spring ($4.8 \pm 4.0 \text{ ng m}^{-3}$), winter ($4.5 \pm 3.2 \text{ ng m}^{-3}$) and summer ($3.8 \pm 3.9 \text{ ng m}^{-3}$). There was a weak but statistically significant negative correlation between the TGM
56 concentration and ambient air temperature ($r = -0.08$) ($p < 0.05$). Although the daytime
57 temperature ($14.7 \pm 10.0 \text{ }^{\circ}\text{C}$) was statistically significantly higher than that in the nighttime
58 ($13.0 \pm 9.8 \text{ }^{\circ}\text{C}$) ($p < 0.05$), the daytime TGM concentration ($5.3 \pm 4.7 \text{ ng m}^{-3}$) was statistically
59 significantly higher than those in the nighttime ($4.7 \pm 4.7 \text{ ng m}^{-3}$) ($p < 0.01$), possibly due to
60 local emissions related to industrial activities and activation of local surface emission
61 sources. The observed $\Delta\text{TGM}/\Delta\text{CO}$ was significantly lower than that of Asian long-range
62 transport, but similar to that of local sources in Korea and in US industrial events suggesting
63 that local sources are more important than that of long-range transport. CPF, CBPF and
64 TPSCF indicated that the main sources of TGM were iron and manufacturing facilities, the
65 hazardous waste incinerators and the coastal areas.

67 **Keywords:** Total gaseous mercury (TGM); co-pollutant; conditional probability function
68 (CPF); conditional bivariate probability function (CBPF); total potential source contribution
69 function (TPSCF)

70 **1. Introduction**

71 Mercury (Hg) is an environmental toxic and bioaccumulative trace metal whose emissions
72 to the environment have considerably increased due to anthropogenic activities such as
73 mining and combustion processes (Pirrone et al., 2013; Streets et al., 2011). Hg can be
74 globally distributed from the sources through atmospheric transport as gaseous elemental
75 form (Bullock et al., 1998; Mason and Sheu, 2002). However, the origins of atmospheric
76 mercury are local and regional (Choi et al., 2009) as well as hemispherical and global
77 (Durnford et al., 2010). In addition to the general background concentration of Hg in the
78 global atmosphere, local Hg emissions contribute to the Hg burden and it contribute to the
79 background concentration much of which represents anthropogenic releases accumulated
80 over the decades (UNEP, 2002).

81 Hg in the atmosphere exists in three major inorganic forms including gaseous elemental
82 mercury (GEM, Hg^0), gaseous oxidized mercury (GOM, Hg^{2+}) and particulate bound
83 mercury (PBM, Hg(p)). GEM which is the dominant form of Hg in ambient air, (>95%) has a
84 relatively long residence time (0.5~2 years) due to its low reactivity and solubility (Schroeder
85 and Munthe, 1998). However, GOM has high water solubility and relatively strong surface
86 adhesion properties (Han et al., 2005), so it has a short atmospheric residence time (~days).
87 PBM is associated with airborne particles such as dust, soot, sea-salt aerosols, and ice crystals
88 (Lu and Schroeder, 2004) and is likely produced, in part, by adsorption of GOM species such
89 as $HgCl_2$ onto atmospheric particles (Gauthard et al., 2005; Lu and Schroeder, 2004; Sakata
90 and Marumoto, 2005; Seo et al., 2012; Seo et al., 2015).

91 Atmospheric Hg released from natural (e.g., volcanoes, volatilization from aquatic and
92 terrestrial environments) (Pirrone et al., 2010; Strode et al., 2007) and anthropogenic sources
93 (e.g., coal combustion, cement production, ferrous and non-ferrous metals manufacturing

94 facilities, waste incineration and industrial boilers) (Pacyna et al., 2010; Pacyna et al., 2006;
95 Pacyna et al., 2003; Pirrone et al., 2010; Zhang et al., 2015) when introduced into terrestrial
96 and aquatic ecosystem through wet and dry deposition (Mason and Sheu, 2002) can undergo
97 various physical and chemical transformations before being deposited. Its lifetime in the
98 atmosphere depends on its reactivity and solubility so that, depending on its form, it can have
99 impacts on local, regional and global scales (Lin and Pehkonen, 1999; Lindberg et al., 2007).
100 A portion of the Hg deposited in terrestrial environments through direct industrial discharge
101 or atmospheric deposition is transported to aquatic system through groundwater and surface
102 water runoff (Miller et al., 2013). A previous study also reported that Hg directly released
103 into terrestrial and aquatic ecosystems from industrial effluent has influenced surface water,
104 sediment and biological tissue (Flanders et al., 2010). Significant spatial variations in
105 atmospheric Hg deposition near urban and industrial areas are due to local anthropogenic
106 sources including municipal waste incinerators, medical waste incinerators, electric power
107 generating facilities and cement kilns (Dvonch et al., 1998), ferrous and non-ferrous metal
108 processing, iron and steel manufacturing facilities, oil and coal combustion (Hoyer et al.,
109 1995), and other forms of industrial combustion (Brown et al., 2015). Miller et al. (2013) also
110 reported that local sources of elemental Hg are typically industrial processes including retort
111 facilities used in the mercury mining industry to convert Hg containing minerals to elemental
112 Hg and chlor-alkali facilities.

113 The annual average national anthropogenic Hg emissions from South Korea in 2007 have
114 been estimated to be 12.8 tons (range 6.5 to 20.2 tons); the major emission sources are coal
115 combustion in thermal power plants (25.8%), oil refineries (25.5%), cement kilns (21%),
116 incinerators (19.3%) including sludge incinerators (4.7%), municipal waste incinerators
117 (MWIs) (3%), industrial waste incinerators (IWIs) (2.7%), hospital/medical/infectious waste

118 incinerators (HMIWIs) (8.8%), and iron manufacturing (7%) (Kim et al., 2010). Global
119 anthropogenic Hg emissions were estimated to be 1960 tons in 2010 with East and Southeast
120 Asia responsible for 777 tons (39.7%) (19.6 tons for Japan and 8.0 tons for South Korea)
121 (AMAP/UNEP, 2013). China is the largest Hg emitting country in the world, contributing
122 more than 800 tons (~ 40%) of the total anthropogenic Hg emissions (UNEP, 2008).

123 Background atmospheric Hg concentrations in the northern hemisphere have decreased
124 since 1996 (Slemr et al., 2003), as measured at the Global Atmosphere Watch (GAW) station
125 at Mace Head, Ireland (Ebinghaus et al., 2011) and at the Canadian Atmospheric Mercury
126 Network (CAMNet) (Temme et al., 2007). In urban areas in South Korea atmospheric TGM
127 concentrations have also decreased over the last few decades due to the reduced fossil fuel
128 (mainly anthracite coal) consumption (Kim et al., 2016; Kim and Kim, 2000). However, this
129 decreasing trend is inconsistent with steady or increasing global anthropogenic Hg emissions
130 since 1990 in the northern hemisphere (Streets et al., 2011; Weigelt et al., 2015; Wilson et al.,
131 2010). A previous study reported that the global anthropogenic Hg emissions are increasing
132 with an average of 1.3% annual growth without including the artisanal and small-scale
133 production sector (Muntean et al., 2014).

134 Receptor models are often used to identify sources of air pollutants and are focused on the
135 pollutants behavior in the ambient environment at the point of impact (Hopke, 2003). In
136 previous studies, conditional probability function (CPF), which utilizes the local wind
137 direction, and potential source contribution function (PSCF), which utilizes longer backward
138 trajectories (typically 3-5 days), combined with concentration data were used to identify
139 possible transport pathways and source locations (Hopke, 2003). While PSCF has been used
140 primarily to identify regional sources, it has also been used to identify local sources (Hsu et
141 al., 2003).

142 The objectives of this study were to characterize the hourly and seasonal variations of
143 atmospheric TGM (the sum of the GEM and the GOM) concentrations, to identify the
144 relationships between TGM and co-pollutant concentrations, and to identify likely source
145 directions and locations of TGM using CPF, conditional bivariate probability function
146 (CBPF) and total PSCF (TPSCF).

147

148 **2. Materials and methods**

149 *2.1. Sampling and analysis*

150 TGM concentrations were measured on the roof of the Korean Federation of
151 Community Credit Cooperatives (KFCCC) building (latitude: 35.992°, longitude: 129.404°,
152 ~10 m above ground) in Pohang city, in Gyeongsangbuk-do, a province in eastern South
153 Korea. Gyeongsangbuk-do has a population of 2.7 million (5% of the total population and the
154 third most populated province in South Korea) and an area of 19,030 km² (19% of the total
155 area of South Korea and the largest province geographically in South Korea). Pohang city has
156 a population of 500,000 (1% of the total population in South Korea) and an area of 605.4 km²
157 (1.1% of the total area in South Korea). It is heavily industrialized with the third largest steel
158 manufacturing facility in Asia and the fifth largest in the world. There are several iron and
159 steel manufacturing facilities including electric and sintering furnaces using coking in
160 Gyeongsangbuk-do including Pohang. In addition, there are several coke plants around the
161 sampling site. The Hyungsan River divides the city into a residential area and the steel
162 complex. Hg emissions data from iron and steel manufacturing, and a hazardous waste
163 incinerator were estimated based on a previous study (Kim et al., 2010) (Fig. 1).

164 TGM concentrations were measured every 5 min during summer (17 August~23 August
165 2012), fall (9 October~17 October 2012), winter (22 January ~29 January 2013), and spring

166 (26 March~3 April 2013) using a mercury vapor analyzer (Tekran 2537B) which has two
167 gold cartridges that alternately collect and thermally desorb mercury. Ambient air at a flow
168 rate of 1.5 L min^{-1} was transported through a 3 m-long heated sampling line (1/4" OD Teflon)
169 in to the analyzer. The sampling line was heated at about 50°C using heat tape to prevent
170 water condensation in the gold traps because moisture on gold surfaces interferes with the
171 amalgamation of Hg (Keeler and Barres, 1999). Particulate matter was removed from the
172 sampling line by a 47 mm Teflon filter.

173

174 *2.2. Meteorological data*

175 Hourly meteorological data (air temperature, relative humidity, and wind speed and
176 direction) were obtained from the Automatic Weather Station (AWS) operated by the Korea
177 Meteorological Administration (KMA) (<http://www.kma.go.kr>) (6 km from the site). Hourly
178 concentrations of NO_2 , O_3 , CO , PM_{10} and SO_2 were obtained from the National Air Quality
179 Monitoring Network (NAQMN) (3 km from the site) (Fig. 1).

180 Meteorological Setting. Fig. S1 shows the frequency of counts of measured wind direction
181 occurrence by season during the sampling period. The predominant wind direction at the
182 sampling site was W (20.9%) and WS (19.2%), and calm conditions of wind speed less than
183 1 m s^{-1} occurred 7.6% of the time. Compared to other seasons, however, the prevailing winds
184 in summer were N (17.0%), NE (16.4%), S (16.4%), and SW (15.8%).

185

186 *2.3. QA/QC*

187 Automated daily calibrations were carried out for the Tekran 2537B using an internal
188 permeation source. Two-point calibrations (zero and span) were separately performed for
189 each gold cartridge. Manual injections were performed prior to every field sampling

190 campaign to evaluate these automated calibrations using a saturated mercury vapor standard.
 191 The relative percent difference (RPD) between automated calibrations and manual injections
 192 was less than 2%. The recovery measured by directly injecting known amounts of four
 193 mercury vapor standards when the sample line was connected to zero air ranged from 92 to
 194 110% ($99.4 \pm 5.2\%$ in average).

195

196 **3. Model descriptions**

197 *3.1. Conditional Probability Function (CPF)*

198 CPF was originally performed to determine which wind directions dominate during high
 199 concentration events to evaluate local source impacts (Ashbaugh et al., 1985). It has been
 200 successfully used in many previous studies (Begum et al., 2004; Kim et al., 2003a; Kim et al.,
 201 2003b; Xie and Berkowitz, 2006; Zhao et al., 2004; Zhou et al., 2004). CPF estimates the
 202 probability that the measured concentration will exceed the threshold criterion for a given
 203 wind direction. The CPF is defined as follows Eq. (1).

204

$$205 \quad CPF_{\Delta\theta} = \frac{m_{\Delta\theta}|_{C \geq x}}{n_{\Delta\theta}} \quad (1)$$

206

207 where, $m_{\Delta\theta}$ is the number of samples from the wind sector θ having concentration C greater
 208 than or equal to a threshold value x , and $n_{\Delta\theta}$ is the total number of samples from wind sector
 209 $\Delta\theta$. In this study, 16 sectors ($\Delta\theta = 22.5^\circ$) were used and calm winds ($\leq 1 \text{ m s}^{-1}$) were excluded
 210 from the analysis. The threshold criterion was set at above the overall average TGM
 211 concentration (5.0 ng m^{-3}). Thus, CPF indicates the potential for winds from a specific
 212 direction to contribute to high air pollution concentrations.

213

214 3.2. Conditional Bivariate Probability Function (CBPF)

215 CBPF couples ordinary CPF with wind speed as a third variable, allocating the measured
 216 concentration of pollutant to cells defined by ranges of wind direction and wind speed rather
 217 than to only wind direction sectors.

218 The CBPF is defined as follows Eq. (2).

219

220
$$CBPF_{\Delta\theta, \Delta u} = \frac{m_{\Delta\theta, \Delta u} | c \geq x}{n_{\Delta\theta, \Delta u}} \quad (2)$$

221

222 where, $m_{\Delta\theta, \Delta u}$ is the number of samples in the wind sector $\Delta\theta$ with wind speed interval Δu
 223 having concentration C greater than a threshold value x , and $n_{\Delta\theta, \Delta u}$ is the total number of
 224 samples in that wind direction-speed interval. The threshold criterion was set at above the
 225 overall average TGM concentration (5.0 ng m⁻³). The extension to the bivariate case can
 226 provide more information on the nature of the sources because different source types such as
 227 stack emission sources and ground-level sources can have different wind speed dependencies
 228 (prominent at high and low wind speed, respectively). More detailed information is described
 229 in a previous study (Uriarreta and Carslaw, 2014).

230

231 3.3. Potential Source Contribution Function (PSCF)

232 The PSCF model has been extensively and successfully used in the previous studies to
 233 identify the likely source areas (Cheng et al., 1993; Han et al., 2004; Hopke et al., 2005; Lai
 234 et al., 2007; Lim et al., 2001; Poissant, 1999; Zeng and Hopke, 1989). The PSCF is a simple
 235 method that links residence time in upwind areas with high concentrations through a
 236 conditional probability field and was originally developed by Ashbaugh et al. (1985). PSCF_{ij}

237 is the conditional probability that an air parcel that passed through the ij th cell had a high
 238 concentration upon arrival at the monitoring site and is defined as the following Eq. (3).

239

240
$$PSCF_{ij} = \frac{m_{ij}}{n_{ij}} \quad (3)$$

241

242 where, n_{ij} is the number of trajectory segment endpoints that fall into the ij -th cell, and m_{ij} is the
 243 number of segment endpoints in the same grid cell (ij -th cell) when the concentrations are higher
 244 than a criterion value as measured at the sampling site.

245 High PSCF values in those grid cells are regarded as possible source locations. Cells including
 246 emission sources can be identified with conditional probabilities close to one if trajectories that
 247 have crossed the cells efficiently transport the released pollutant to the receptor site. Therefore,
 248 the PSCF model provides a tool to map the source potentials of geographical areas.

249 The criterion value of PSCF for TGM concentration was set at above the overall average
 250 concentration (5.0 ng m^{-3}) to identify the emission sources associated with high TGM
 251 concentrations and provide a better estimation and resolution of source locations during the
 252 sampling periods. The geographic area covered by the computed trajectories was divided into
 253 an array of 0.05° latitude by 0.05° longitude grid cells. As will be discussed in Section 5.3, 24
 254 h backward trajectories starting at every hour at a height of 10, 50, and 100 m above ground
 255 level were computed using the vertical velocity model because local sources are more
 256 important than that of long-range transport in this study (It should be noted that PSCF results
 257 using 48 h backward trajectories had similar results as the 24 h backward trajectories). Each
 258 trajectory was terminated if they exit the model top (5,000m), but advection continues along
 259 the surface if trajectories intersect the ground. To generate horizontally highly resolved
 260 meteorological inputs for trajectory calculations, the Weather Research and Forecast (WRF)

261 model was used to generate a coarse domain at a resolution of 27 km and a nested domain at
 262 a horizontal resolution of 9 km, which geographically covers northeast Asia and the southern
 263 part of the Korean Peninsula, respectively. The nested domain has 174 columns in the east-
 264 west direction and 114 rows in the north-south direction. PSCF was calculated with 9 km
 265 meteorological data.

266 In this study, TPSCF which incorporates probability from above different starting
 267 heights was calculated since backward trajectories starting at different heights traverse
 268 different distances and pathways, thus providing information that cannot be obtained from a
 269 single starting height (Cheng et al., 1993).

270 Previous studies suggest that there are increasing uncertainties as backward trajectory
 271 distances increase (Stohl et al., 2002) and that PSCF modeling is prone to the trailing effect is
 272 which locations upwind of sources are also identified as potential sources (Han et al., 2004).
 273 An alternative to back trajectory calculations in the interpretation of atmospheric trace
 274 substance measurements (Stohl et al., 2002) although this technique does not provide much
 275 information on source locations.

276 Generally, PSCF results show that the potential sources covered wide areas instead of
 277 indicating individual sources due to the trailing effect. The trailing effect appears since PSCF
 278 distributes a constant weight along the path of the trajectories. To minimize the effect of
 279 small n_{ij} (the number of trajectory segment endpoints that fall into the ij -th cell) values,
 280 resulting in high TPSCF values with high uncertainties, an arbitrary weight function $W(n_{ij})$
 281 was applied to down-weight the PSCF values for the cell in which the total number of end
 282 points was less than three times the average value of the end points (Choi et al., 2011; Heo et
 283 al., 2009; Hopke et al., 1995; Polissar et al., 2001). The TPSCF value for a grid cell was
 284 defined with following Eq. (4).

285

$$286 \quad P(TPSCF_{ij}) = \frac{P(m_{ij})_{10m} + P(m_{ij})_{50m} + P(m_{ij})_{100m}}{P(n_{ij})_{10m} + P(n_{ij})_{50m} + P(n_{ij})_{100m}} \times W \quad (4)$$

287

288 where,

$$289 \quad W(n_{ij}) = \begin{cases} 1.0, & 3n_{ave} < n_{ij} \\ 0.8, & 2n_{ave} < n_{ij} \leq 3n_{ave} \\ 0.6, & n_{ave} < n_{ij} \leq 2n_{ave} \\ 0.4, & 0.5n_{ave} < n_{ij} \leq n_{ave} \\ 0.2, & n_{ij} \leq 0.5n_{ave} \end{cases}$$

290

291 **4. Clean Air Policy Support System (CAPSS) data**

292 In this study, the Korean National Emission Inventory estimated using Clean Air Policy
 293 Support System (CAPSS) data developed by the National Institute of Environmental
 294 Research (NIER) were used (<http://airemiss.nier.go.kr/main.jsp> (accessed December 09,
 295 2015)). The CAPSS is the national emission inventory system for the air pollutants (CO,
 296 NOx, SOx, TSP, PM₁₀, PM_{2.5}, VOCs and NH₃) which utilizes various national, regional and
 297 local statistical data collected from about 150 organizations in Korea. In CAPSS, the Source
 298 Classification Category (SCC) excluding fugitive dust and biomass burning based on the
 299 European Environment Agency's (EEA) CORe Inventory of AIR emissions was classified
 300 into the following four levels (EMEP/CORINAIR) (NIER, 2011).

301 (1) The upper level (SCC1): 11 source categories ,

302 (2) The intermediate level (SCC2): 42 source categories and

303 (3) The lower level (SCC3): 173 source categories

304

305 The sectoral contributions of emissions of South Korea, Gyeongsangbuk-do and Pohang
306 for CO, NOx, SOx, TSP, PM₁₀, PM_{2.5}, VOC and NH₃ are shown in [Fig. S2](#) (See SI for
307 details).

308 More detailed information about SCCs in CAPSS is described in [Table S1](#).

309

310 5. Results and Discussions

311 5.1. General characteristics of TGM

312 The seasonal distributions of TGM were characterized by large variability during each
313 sampling period ([Fig. 2](#)). The average concentration of TGM during the complete sampling
314 period was $5.0 \pm 4.7 \text{ ng m}^{-3}$ (range: 1.0-79.6 ng m^{-3}). This is significantly higher than the
315 Northern Hemisphere background concentration ($\sim 1.5 \text{ ng m}^{-3}$) (Sprovieri et al., 2010) and
316 those measured in China, in Japan and other locations in Korea, however [lower than those](#)
317 [measured at Changchun, Gui Yang and Nanjing in China](#) ([Table 1](#)). The median TGM
318 concentration was 3.6 ng m^{-3} which was much lower than that of the average, suggesting that
319 there were some extreme pollution episodes with very high TGM concentrations.

320 The TGM concentration follows a typical log-normal distribution ([Fig. S3](#)). The range of 2
321 to 5 ng m^{-3} dominated the distribution, accounting for more than half of the total number of
322 samples (60.8%). The maximum frequency of 28.1% occurred between 2 and 3 ng m^{-3} .
323 Extremely high TGM concentration events ($>20 \text{ ng m}^{-3}$) were also observed (1.7% of the
324 time).

325

326

327

328 5.2. Seasonal variations

329 The TGM concentration was statistically significantly higher in fall ($6.7 \pm 6.4 \text{ ng m}^{-3}$) ($p <$
 330 0.01), followed by spring ($4.8 \pm 4.0 \text{ ng m}^{-3}$), winter ($4.5 \pm 3.2 \text{ ng m}^{-3}$) and summer (3.8 ± 3.9
 331 ng m^{-3}) (Table 2). The highest concentrations (TGM $> 10 \text{ ng m}^{-3}$) were measured more
 332 frequently in fall (24.7%), and the lowest concentrations (TGM $< 3 \text{ ng m}^{-3}$) mainly occurred
 333 in summer (49.7%). The low TGM concentration in summer is likely because increased
 334 mixing height (Friedli et al., 2011), and gas phase oxidation (Choi et al., 2013; Huang et al.,
 335 2010; Lynam and Keeler, 2006) at higher temperatures particularly at this sampling site
 336 which is close to the ocean (2 km) where oxidation involving halogens may be enhanced
 337 (Holmes et al., 2009; Lin et al., 2006). The high TGM concentrations in fall was due to
 338 different wind direction (see Fig. S1), sources, relationships with other pollutants and
 339 meteorological conditions. More detailed information can be found in Section 5.4.

340 The average concentrations of NO₂, O₃, CO, PM₁₀ and SO₂ during the complete sampling
 341 period were $23.1 \pm 10.8 \text{ ppbv}$, $24.6 \pm 12.5 \text{ ppbv}$, $673.7 \pm 487.3 \text{ ppbv}$, $55.5 \pm 26.4 \text{ } \mu\text{g m}^{-3}$ and
 342 $6.7 \pm 4.3 \text{ ppbv}$, respectively. NO₂, O₃, CO, PM₁₀ and SO₂ concentrations were highest in
 343 spring (Table 2). There was a statistically significant positive correlation between the TGM
 344 and PM₁₀ ($r = 0.10$) ($p < 0.01$). However, the TGM concentration was not significantly
 345 correlated with NO₂, CO or SO₂ concentrations, suggesting that combustion associated with
 346 space heating was not a significant source of TGM (Choi et al., 2009).

347

348 5.3. Relationship between TGM and CO

349 CO has a significant anthropogenic source and is considered to be an indicator of
 350 anthropogenic emissions (Mao et al., 2008). Previous studies reported that TGM and CO

351 have a strong correlation because they have similar emission sources (combustion processes)
352 and similar long atmospheric residence times (Weiss-Penzias et al., 2003).

353 There was a weak positive correlation between TGM and CO in this study ($r = 0.04$) ($p =$
354 0.27). However there was a statistically significant correlation between TGM and CO in
355 winter ($r = 0.25$) ($p < 0.05$), suggesting that TGM and CO were affected by similar, possibly
356 distant, anthropogenic emission sources in winter.

357 On the other hand, there were no statistically significant correlations between TGM and
358 CO in spring ($r = 0.02$) ($p = 0.78$), in summer ($r = 0.13$) ($p = 0.08$), or in fall ($r = -0.03$) ($p =$
359 0.69), indicating that TGM and CO were affected by different anthropogenic emission
360 sources in these seasons.

361 Previous studies identified the long-range transport of mercury using the $\Delta\text{TGM}/\Delta\text{CO}$
362 enhancement ratio (Choi et al., 2009; Jaffe et al., 2005; Kim et al., 2009; Weiss-Penzias et al.,
363 2003; Weiss-Penzias et al., 2006). Kim et al. (2009) and Choi et al. (2009) investigated high
364 concentration events which were defined as at least a 10 h period with hourly average TGM
365 and CO concentrations higher than the average monthly TGM and CO concentrations. They
366 reported that long-range transport events were characterized by high values of TGM/CO ratio
367 ($\Delta\text{TGM}/\Delta\text{CO}$) ($0.0052\text{-}0.0158 \text{ ng m}^{-3} \text{ ppb}^{-1}$) and high correlations ($r^2 > 0.5$), whereas local
368 events showed low $\Delta\text{TGM}/\Delta\text{CO}$ ($0.0005 \text{ ng m}^{-3} \text{ ppb}^{-1}$ in average) and weak correlations ($r^2 <$
369 0.5).

370 The observed $\Delta\text{TGM}/\Delta\text{CO}$ was $0.0001 \text{ ng m}^{-3} \text{ ppb}^{-1}$ in spring, $0.0005 \text{ ng m}^{-3} \text{ ppb}^{-1}$ in
371 summer, $-0.0007 \text{ ng m}^{-3} \text{ ppb}^{-1}$ in fall, $0.0011 \text{ ng m}^{-3} \text{ ppb}^{-1}$ in winter, which are significantly
372 lower than that indicative of Asian long-range transport ($0.0046\text{-}0.0056 \text{ ng m}^{-3} \text{ ppb}^{-1}$) (Friedli

373 et al., 2004; Jaffe et al., 2005; Weiss-Penzias et al., 2006), suggesting that local sources are
 374 more important than that of long-range transport in this study. The $\Delta\text{TGM}/\Delta\text{CO}$ in winter
 375 ($0.0011 \text{ ng m}^{-3} \text{ ppb}^{-1}$) was similar to that of a site impacted by local sources in Korea (Kim et
 376 al., 2009) and in US industrially related events ($0.0011 \text{ ng m}^{-3} \text{ ppb}^{-1}$) (Weiss-Penzias et al.,
 377 2007).

378 There are also uncertainties from the potential mixing between Hg associated with long-
 379 range transported airflows and local air making it difficult to distinguish between distant and
 380 local source impacts. However, it is possible that the one-week sampling period in each
 381 season did not capture the long-range transport events, and more can be learned using a larger
 382 dataset than just using the one-week sampling period to confirm these results.

383

384 *5.4. Diurnal variations*

385 Diurnal variations of TGM (Fig. 3), co-pollutants concentrations, and meteorological
 386 data were observed (Fig. S4). TGM, O₃, CO, SO₂, and temperature in the daytime (06:00-
 387 18:00) were higher than those in the nighttime (18:00-06:00) ($p < 0.05$) except PM₁₀ ($p =$
 388 0.09) (Fig. S5). However, NO₂ during the nighttime because of relatively lower
 389 photochemical reactivity with O₃ was higher than that in daytime ($p < 0.05$) (Adame et al.,
 390 2012).

391 The daytime TGM concentration ($5.3 \pm 4.7 \text{ ng m}^{-3}$) was higher than that in the nighttime
 392 ($4.7 \pm 4.7 \text{ ng m}^{-3}$) ($p < 0.01$), which was similar to several previous studies (Cheng et al.,
 393 2014; Gabriel et al., 2005; Nakagawa, 1995; Stamenkovic et al., 2007) but different than
 394 another studies (Lee et al., 1998). Previous studies reported that this different is due to local
 395 sources close to the sampling site (Cheng et al., 2014; Gabriel et al., 2005), a positive
 396 correlation between TGM concentration and ambient air temperature (Nakagawa, 1995) and

397 increased traffic (Stamenkovic et al., 2007). However, another study suggested that the higher
398 TGM concentration during the night was due to the shallowing of the boundary layer, which
399 concentrated the TGM near the surface (Lee et al., 1998).

400 In a previous study the daytime TGM concentration was relatively lower than that in the
401 nighttime because the sea breeze transported air containing low amounts of TGM from the
402 ocean during the daytime whereas the land breeze transported air containing relatively high
403 concentrations of TGM from an urban area during the nighttime (Kellerhals et al., 2003).

404 Although it is possible that the land-sea breeze may affect diurnal variations in TGM
405 concentrations since the sampling site was near the ocean and lower TGM were also observed
406 during the daytime, the higher concentrations in the daytime than those in nighttime were due
407 to local emission sources because the daytime temperature ($14.7 \pm 10.0^{\circ}\text{C}$) was statistically
408 significantly higher than that in the nighttime ($13.0 \pm 9.8^{\circ}\text{C}$) (t-test, $p < 0.05$) and there was a
409 weak but statistically significant negative correlation between TGM concentration and
410 ambient air temperature ($r = -0.08$) ($p < 0.05$). In addition, there are several known Hg
411 sources such as iron and steel manufacturing facilities including electric and sintering
412 furnaces using coking between the sampling site and the ocean.

413 As shown in Fig. 3 and Fig. S4, there was a weak but negative relationship between the
414 TGM concentrations and O_3 concentrations ($r = -0.18$) ($p < 0.01$), suggesting that oxidation
415 of GEM in the oxidizing atmosphere during periods of strong atmospheric mixing was
416 partially responsible for the diurnal variations of TGM concentrations. In addition, oxidation
417 of GEM by bromine species in the coastal area (Obrist et al., 2011) or by chloride radicals in
418 marine boundary layer (Laurier et al., 2003) might play a significant role. If oxidation of
419 GEM occurred, GOM concentrations would increase. However there are uncertainties on the

420 net effects on TGM (the sum of the GEM and the GOM) since we did not measure GOM
421 concentrations.

422 TGM concentration was negatively correlated with ambient air temperature ($r = -0.08$)
423 ($p < 0.05$) because high ambient air temperature in the daytime will increase the height of the
424 boundary layer and dilute the TGM, and the relatively lower boundary layer at nighttime
425 could concentrate the TGM in the atmosphere (Li et al., 2011). Although there was a
426 statistically significant negative correlation between the TGM concentration and ambient air
427 temperature, there was a rapid increase in TGM concentration between 06:00-09:00 when
428 ambient temperatures also increased possibly due to local emissions related to industrial
429 activities, increased traffic, and activation of local surface emission sources. Similar patterns
430 were found in previous studies (Li et al., 2011; Stamenkovic et al., 2007). Nonparametric
431 correlations revealed that there is a weak positive correlation between TGM and ambient air
432 temperature ($r_s = 0.11, p=0.27$) between 06:00-09:00. The TGM concentration was
433 negatively correlated with O_3 ($r_s = -0.33, p<0.01$) but positively correlated with NO_2 ($r_s =$
434 $0.21, p<0.05$), suggesting that the increased traffic is the main source of TGM during these
435 time periods.

436 Compared to other seasons, significantly different diurnal variations of TGM were
437 observed in fall. The daytime TGM concentrations in fall were similar to those in other
438 seasons, however, the nighttime TGM concentrations in fall were much higher than other
439 seasons. As described earlier in Section 5.2, the high TGM concentrations in fall was
440 possibly due to the relationship between other pollutants and meteorological conditions as
441 well as different wind direction and sources. The nighttime TGM concentrations in fall were
442 simultaneously positively correlated with PM_{10} ($r=0.26$) ($p<0.05$) and CO ($r=0.21$) ($p<0.05$)

443 concentrations and wind speed ($r=0.35$) ($p<0.01$), suggesting that the combustion process is
444 an important source during this period.

445 TGM generally showed a consistent increase in the early morning (06:00-09:00) and a
446 decrease in the afternoon (14:00-17:00), similar to previous studies (Dommergue et al., 2002;
447 Friedli et al., 2011; Li et al., 2011; Liu et al., 2011; Mao et al., 2008; Shon et al., 2005; Song
448 et al., 2009; Stamenkovic et al., 2007). Significantly different diurnal patterns have been
449 observed at many suburban sites with the daily maximum occurring in the afternoon (12:00-
450 15:00), possibly due to local emission sources and transport (Fu et al., 2010; Fu et al., 2008;
451 Kuo et al., 2006; Wan et al., 2009). Other studies in Europe reported that TGM
452 concentrations were relatively higher early in the morning or at night possibly due to mercury
453 emissions from surface sources that accumulated in the nocturnal inversion layer (Lee et al.,
454 1998; Schmolke et al., 1999).

455 Based on the above results, the diurnal variations in TGM concentration are due to a
456 combination of: 1) reactions with an oxidizing atmosphere, 2) changes in ambient
457 temperature and 3) local emissions related to industrial activities. To supplement these
458 conclusions CPF and CBPF were used to identify source directions and TPSCF was used to
459 identify potential source locations.

460

461 5.5. CPF, CBPF and TPSCF results of TGM

462 Conventional CPF, CBPF and TPSCF plots for TGM concentrations higher than the
463 average concentration show high source probabilities to the west in the direction of large steel
464 manufacturing facilities and waste incinerators (Fig. 4). The CPF only shows high
465 probabilities from the west and provides no further information, however, the CBPF shows
466 groups of sources with the high probabilities from the west and the northeast. CBPF shows

467 that the high probabilities from the west occurred under high wind speed ($> 3 \text{ m s}^{-1}$)
468 indicative of emissions from stacks as well as low wind speed ($\leq 3 \text{ m s}^{-1}$) indicative of non-
469 buoyant ground level sources (Urias-Tellaetxe and Carslaw, 2014).

470 As described in Section 5.3, correlations between TGM and CO revealed that TGM and
471 CO were affected by similar anthropogenic emission sources in winter but affected by
472 different sources in spring, summer and fall, which is supported by [Fig. S6](#) which shows
473 significantly different seasonal patterns of CPF and CBPF for TGM concentrations.
474 However, compared to [Fig. 4](#), the CPF and CBPF patterns in fall were similar to those during
475 the whole sampling periods. Especially, the nighttime TGM concentration in fall was
476 simultaneously positively correlated with PM_{10} ($r=0.26$) ($p<0.05$) and CO ($r=0.21$) ($p<0.05$)
477 concentrations and wind speed ($r=0.35$) ($p<0.01$), indicating that the combustion process
478 from the west is an important source during this period.

479 Since TGM showed a significant correlation with CO ($r=0.25$) ($p<0.05$) and showed a
480 weak positive correlation with PM_{10} ($r=0.08$) ($p=0.33$) in winter with high wind speed,
481 combustion sources from the west are likely partially responsible for this result.

482 TPSCF identified the likely sources of TGM as the iron and manufacturing facilities and
483 the hazardous waste incinerators which are located to the west from the sampling site. A
484 previous study reported that the waste incinerators (9%) and iron and steel manufacturing
485 (7%) were relatively high Hg emissions sources in Korea (Kim et al., 2010). Waste
486 incinerators emissions were due to the high Hg content in the waste (Lee et al., 2004).
487 Emissions from iron and steel manufacturing are due to the numerous electric and sintering
488 furnaces using coking which emits relatively high mercury concentrations (Lee et al., 2004)
489 in Gyeongsangbuk-do including Pohang. There are several coke plants around the sampling
490 site (http://www.poscoenc.com/upload/W/BUSINESS/PDF/ENG_PLANT_2_1_3_5.pdf

491 (accessed December 09, 2015)). They are essential parts of the iron and steel manufacturing,
492 and the major source of atmospheric mercury related to the iron and steel manufacturing is
493 from coke production (Pacyna et al., 2006).

494 The coastal areas east of the sampling site where there are large ports were also identified
495 as the likely source areas of TGM. A previous study reported that the emissions of gaseous
496 and particulate pollutants were high during vehicular operations in port areas and from
497 marine vessel and launches (Gupta et al., 2002). Another possibility is that significant amount
498 of GEM are emitted from the ocean surface because of photo-chemically and
499 microbiologically mediated photo-reduction of dissolved GOM (Amyot et al., 1994; Zhang
500 and Lindberg, 2001). The northeast direction including the East Sea was also identified as
501 potential source areas likely because this is an area with lots of domestic passenger ships
502 routes. The south from the sampling site was also identified as a likely source area of TGM
503 where Ulsan Metropolitan City, South Korea's seventh largest metropolis with a population
504 of over 1.1 million is located. It includes a large petrochemical complex known as a TGM
505 source (Jen et al., 2013).

506

507 **Conclusions**

508 During the sampling periods, the average TGM concentration was higher than the Northern
509 Hemisphere background concentration, however, considerably lower than those near urban
510 areas in China and higher than those in Japan and other locations in Korea. The median
511 concentration of TGM was much lower than that of the average, suggesting that there were
512 some extreme pollution episodes with very high TGM concentrations. The TGM
513 concentration was highest in fall, followed by spring, winter and summer. The high TGM
514 concentration in fall is due to transport from different wind directions than during the other
515 periods. The low TGM concentration in summer is likely due to increased mixing height and
516 gas phase oxidation at higher temperatures particularly at this sampling site which is close to
517 the ocean (2 km) where oxidation involving halogens may be enhanced.

518 TGM consistently showed a diurnal variation with a maximum in the early morning
519 (06:00-09:00) and minimum in the afternoon (14:00-17:00). Although there was a statistically
520 significant negative correlation between the TGM concentration and ambient air temperature,
521 the daytime TGM concentration was higher than those in the nighttime, suggesting that local
522 emission sources are important. There was a negative relationship between the TGM
523 concentrations and O₃ concentrations, indicating that the oxidation was partially responsible
524 for the diurnal variations of TGM concentrations. The observed $\Delta\text{TGM}/\Delta\text{CO}$ was
525 significantly lower than that indicative of Asian long-range transport, suggesting that local
526 sources are more important than that of long-range transport. CPF only shows high
527 probabilities to the west from the sampling site where there are large steel manufacturing
528 facilities and waste incinerators. However, CBPF and TPSCF indicated that the dominant
529 sources of TGM were the hazardous waste incinerators and the coastal areas in the northeast

530 as well as the iron and manufacturing facilities in the west. The domestic passenger ships
531 routes in the East Sea were also identified as possible source areas.

532

533 **Author contribution**

534 Yong-Seok Seo conducted a design of the study, the experiments and analysis of data, wrote
535 the initial manuscript, and finally approved the final manuscript. Seung-Pyo Jeong, Eun Ha
536 Park, Tae Young Kim, Hee-Sang Eum, Dae Gun Park, Eunhye Kim, Jaewon Choi and Jeong-
537 Hun Kim conducted the experiments, analysis of data, and finally approved the final
538 manuscript. Thomas M. Holsen, Young-Ji Han and Eunhwa Choi and Soontae Kim
539 conducted interpretation of the results, revision of the initial manuscript, and finally approved
540 the final manuscript. Seung-Muk Yi conducted a design of the study, acquisition of data of the
541 study, interpretation of data, and revision of the initial manuscript, and finally approved the final
542 manuscript.

543

544 **Acknowledgments**

545 We thank National Institute of Environmental Research (NIER) for providing CAPSS data.
546 This work was supported by Brain Korea 21 (BK21) Plus Project (Center for Healthy
547 Environment Education and Research) through the National Research Foundation (NRF) of
548 Korea and Korea Ministry of Environment (MOE) as “the Environmental Health Action
549 Program”.

550

551 **Table List**

552 Table 1. Comparison with previous studies for TGM concentrations.

553 Table 2. Summary of atmospheric concentrations of TGM and co-pollutants, and
554 meteorological data.

555

556 **Figure List**

557 Fig. 1. The location of sampling site in this study ((a) South Korea, (b) Gyeongsangbuk-do
558 and (c) Pohang).

559 Fig. 2. Time-series of TGM concentrations in this study.

560 Fig. 3. The diurnal variations of TGM concentrations during the sampling periods.

561 Fig. 4. CPF, CBPF and TPSCF plots for TGM higher than average concentration.

562

Table 1. Comparison with previous studies for TGM concentrations.

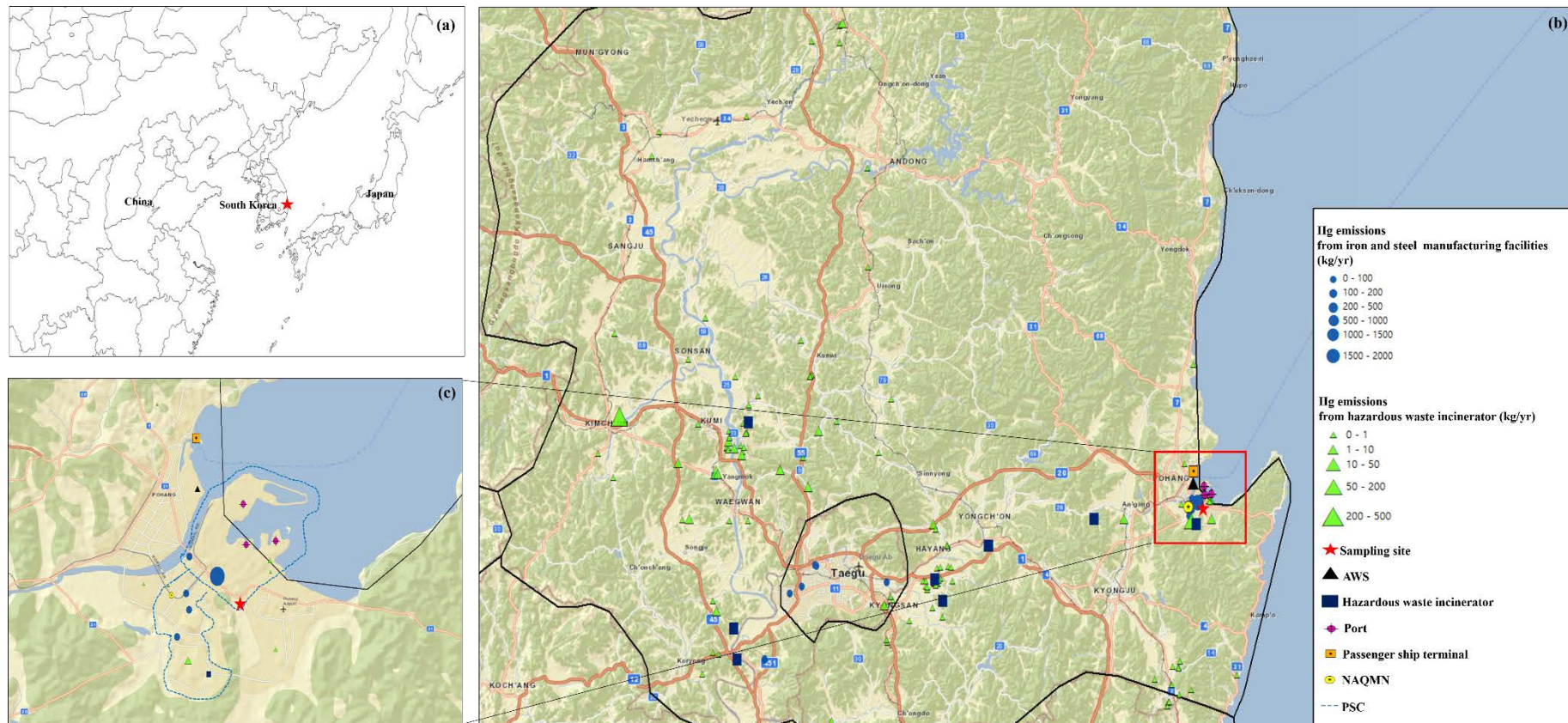
Country	Location	Sampling period	TGM conc. (ng m^{-3})	Classifications	Reference
China	Mt. Hengduan, Qinghai-Tibet Plateau	Jul. 2010 ~ Oct. 2010	2.5	Remote	Fu et al. (2015)
China	Nanjing, Jiangsu	Jan. 2011 ~ Oct. 2011	7.9	Urban	Hall et al. (2014)
China	Mt. Dinghu, Guangdong	Oct. 2009 ~ Apr. 2010	5.1	Rural	Chen et al. (2013)
China	Guangzhou, Guangdong	Nov. 2010 ~ Nov. 2011	4.6	Urban	Chen et al. (2013)
China	Gui Yang, Guizhou	Jan. 2010 ~ Feb. 2010	8.4	Urban	Feng et al. (2004)
China	Changchun, Jilin	Jul. 1999 ~ Jul. 2000	13.5-25.4	Urban	Fang et al. (2004)
Japan	Fukuoka	Jun. 2012 ~ May 2013	2.33	Urban	Marumoto et al. (2015)
Japan	Tokai-mura	Oct. 2005 ~ Aug. 2006	3.8	Suburban	Osawa et al. (2007)
Japan	Tokyo	Apr. 2000 ~ Mar. 2001	2.7	Urban	Sakata and Marumoto (2002)
Korea	Seoul	1987 ~ 2013	3.7	Urban	Kim et al. (2016)
Korea	Gangwon-do, Chuncheon	2006 ~ 2009	2.1	Rural	Han et al. (2014)
Korea	Seoul	Feb. 2005 ~ Feb. 2006	3.2	Urban	Kim et al. (2009)
Korea	Seoul	Feb. 2005 ~ Dec. 2006	3.4	Urban	Choi et al. (2009)
Korea	Seoul	19 Sep. 1997 ~ 29 Sep. 1997 27 May. 1998 ~ 18 Jun. 1998	3.6	Urban	Kim and Kim (2001)
Korea	Gyeongsangbuk-do, Pohang	17 Aug. 2012 ~ 23 Aug. 2012 9 Oct. 2012 ~ 17 Oct. 2012 22 Jan. 2013 ~ 29 Jan. 2013 26 Mar. 2013 ~ 3 Apr. 2013	5.0	Urban	This study

563

564 **Table 2.** Summary of atmospheric concentrations of TGM and co-pollutants, and meteorological data. Note that TGM was measured every 5-
 565 min, and other pollutants and meteorological data were measured every 1-hour.

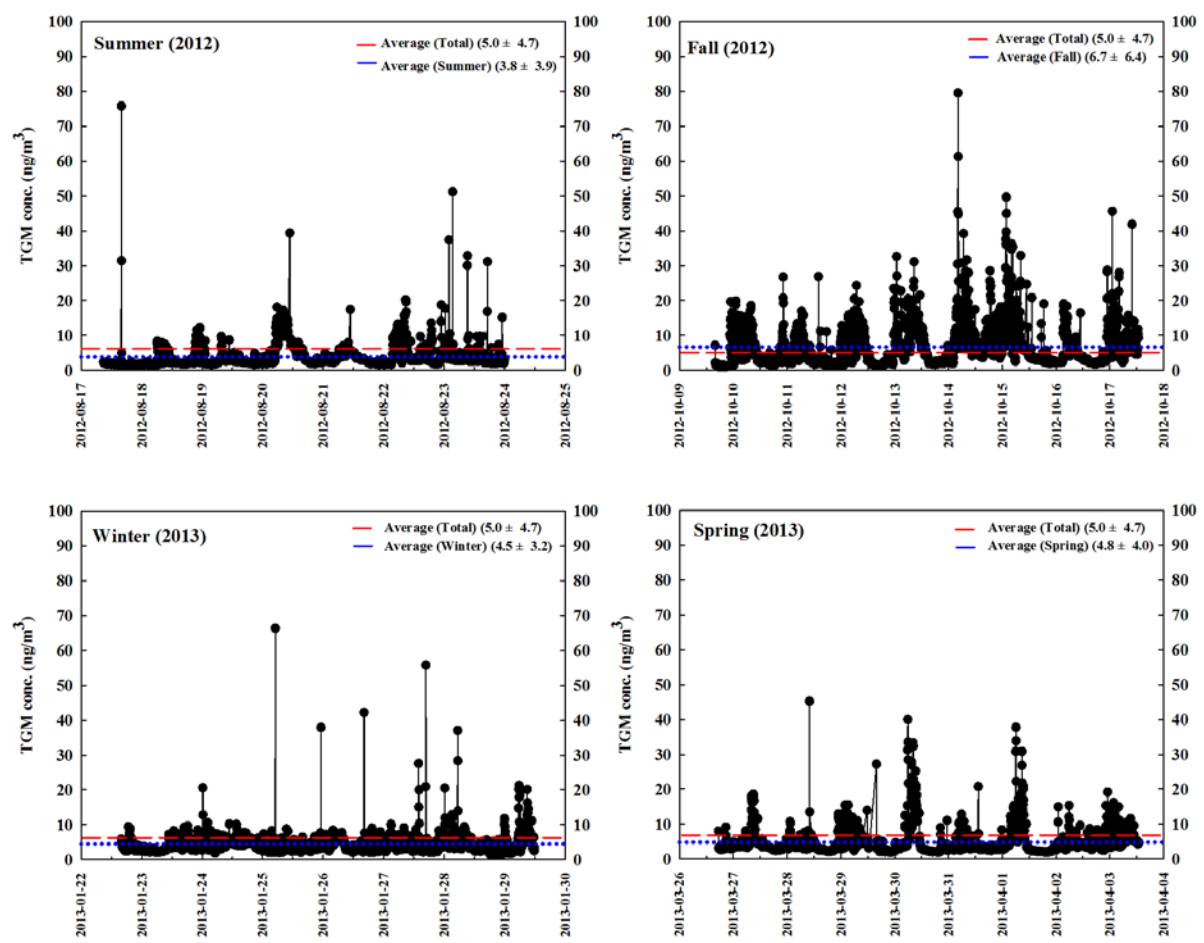
		TGM (ng m ⁻³)	NO ₂ (ppb)	O ₃ (ppb)	CO (ppb)	PM ₁₀ (μ g m ⁻³)	SO ₂ (ppb)	Temperature (°C)	Wind speed (m s ⁻¹)	Humidity (%)	Solar radiation (MJ m ⁻²)
Spring	N	2139	189	215	215	215	215	216	216	216	216
	Average	4.8 ± 4.0	25.3 ± 9.0	29.4 ± 14.2	766.5 ± 505.2	70.1 ± 26.0	7.6 ± 3.8	10.5 ± 4.2	2.2 ± 1.2	56.2 ± 16.8	0.82 ± 1.09
	Range	1.9 – 45.3	8 – 55	2 – 58	300 – 3100	28 – 204	5 – 35	1.1 – 21.6	0.4 – 6.2	19.0 – 94.0	0 – 3.44
Summer	N	1863	187	188	187	188	188	186	180	186	141
	Average	3.8 ± 3.9	18.3 ± 9.2	18.9 ± 10.1	697.3 ± 689.7	35.1 ± 15.8	6.5 ± 6.2	26.6 ± 4.2	2.2 ± 1.1	82.5 ± 13.9	0.40 ± 0.69
	Range	1.2 – 75.9	4 – 44	5 – 48	200 – 3300	12 – 87	2 – 27	19.7 – 34.1	0.1 – 6.4	43 – 98	0 – 2.92
Fall	N	2226	212	212	212	212	211	216	216	216	216
	Average	6.7 ± 6.4	25.0 ± 7.8	23.7 ± 13.1	662.7 ± 350.2	58.1 ± 17.8	5.3 ± 3.5	17.4 ± 3.2	2.1 ± 0.8	54.5 ± 14.7	0.62 ± 0.90
	Range	1.0 – 79.6	9 – 53	6 – 69	300 – 2900	20 – 145	3 – 39	11.7 – 25.2	0.5 – 4.5	12 – 79	0 – 2.90
Winter	N	1917	188	187	188	188	186	192	192	192	192
	Average	4.5 ± 3.2	23.5 ± 14.7	26.1 ± 8.7	556.4 ± 298.9	56.3 ± 30.5	7.4 ± 2.5	1.1 ± 4.3	2.8 ± 1.1	46.3 ± 24.5	0.43 ± 0.71
	Range	1.3 – 66.4	5 – 74	1 – 41	200 – 2400	18 – 161	5 – 24	-0.65 – 10.1	0.5 – 6.0	11 – 90	0 – 2.34
Total	N	8145	776	802	802	803	800	810	804	810	765
	Average	5.0 ± 4.7	23.1 ± 10.8	24.6 ± 12.5	673.7 ± 487.3	55.5 ± 26.4	6.7 ± 4.3	13.8 ± 9.9	2.3 ± 1.1	59.4 ± 22.1	0.59 ± 0.90
	Range	1.0 – 79.6	4 – 74	1 – 69	200 – 3300	12 – 204	2 – 39	-6.5 – 34.1	0.1 – 6.4	11 – 98	0 – 3.44

566



567

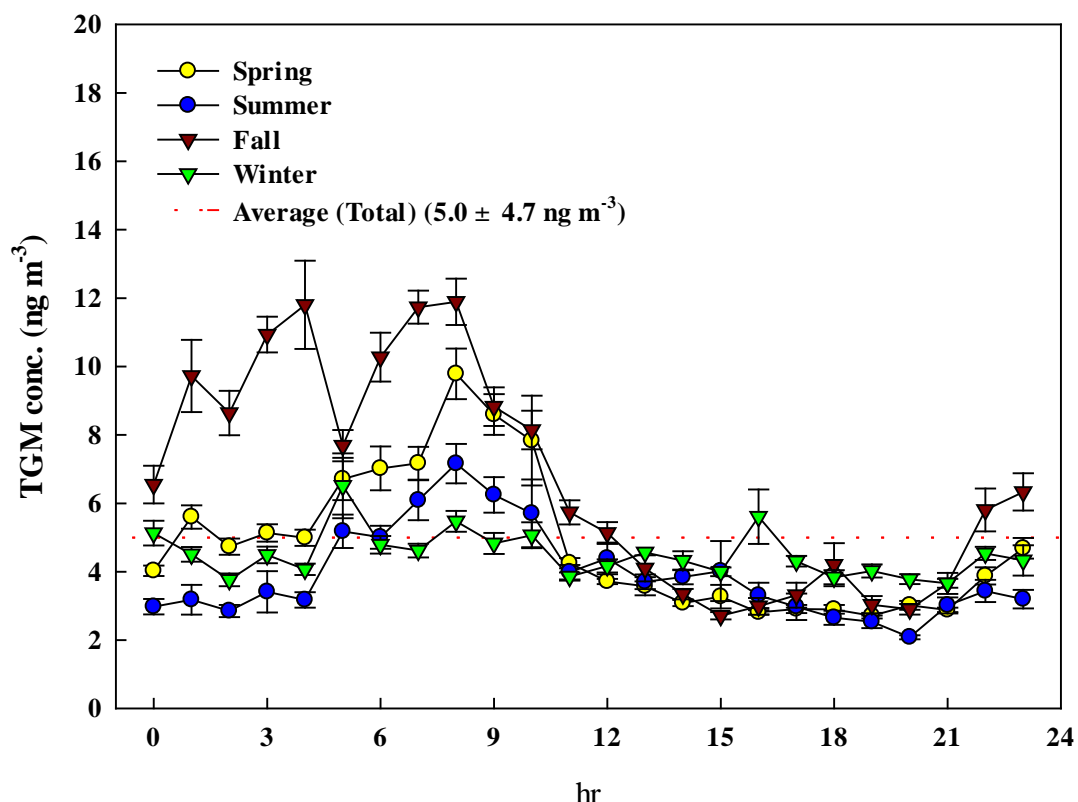
Fig. 1. The location of sampling site in this study ((a) South Korea, (b) Gyeongsangbuk-do and (c) Pohang). AWS, NAQMN and PSC represent Automatic Weather Station, National Air Quality Monitoring Network and Pohang Steel Complex, respectively.



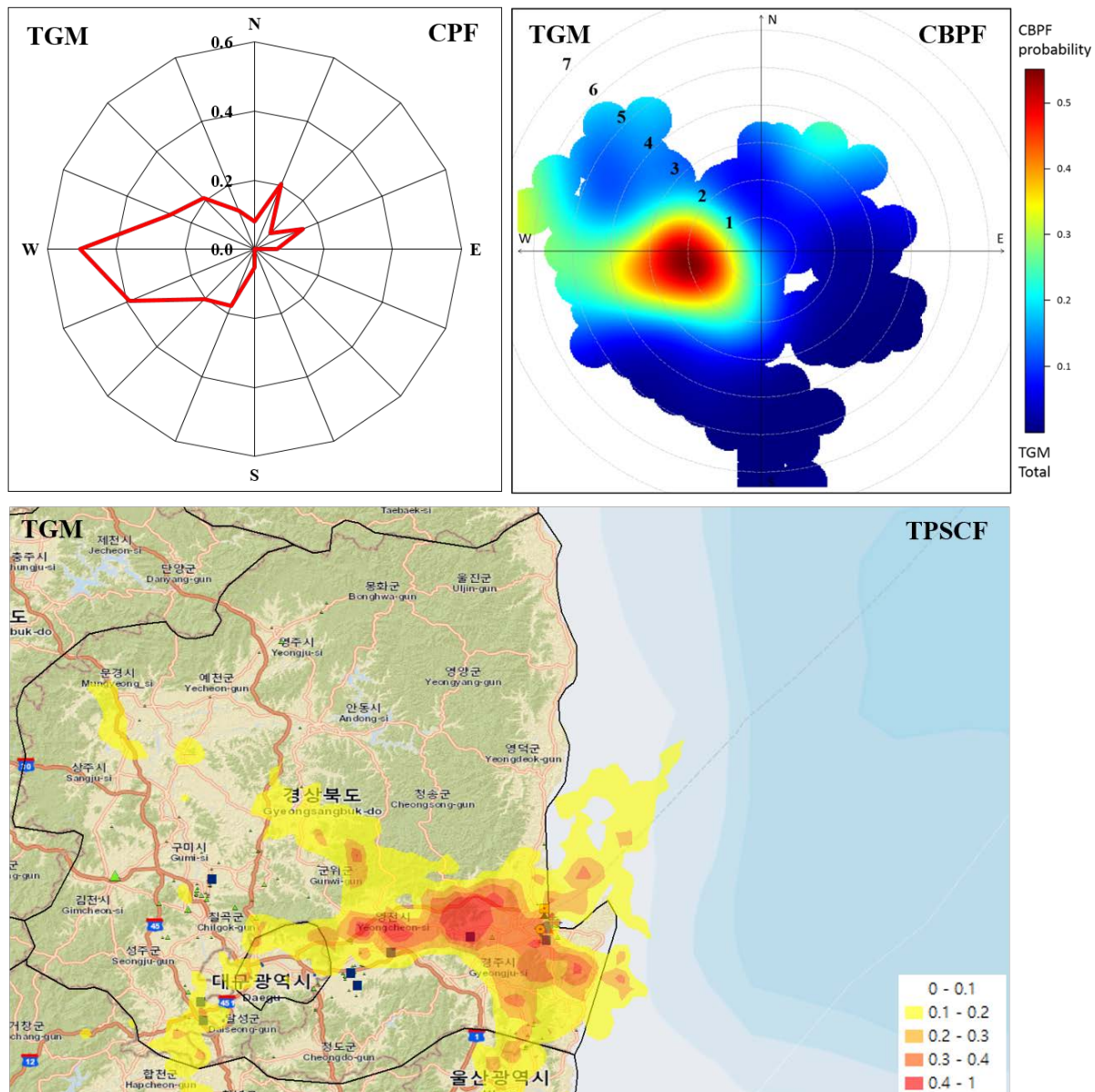
568

569

Fig. 2. Time-series of TGM concentrations in this study.



570
571 **Fig. 3.** The diurnal variations of TGM concentrations during the sampling periods.
572 The error bars represent standard error.



573
574
575
576

Fig. 4. CPF, CBPF and TPSCF plots for TGM higher than average concentration. The radial axes of CPF and CBPF are the probability and the wind speed (m s^{-1}), respectively.

577 **References**

578

579 Adame, J., Notario, A., Villanueva, F., and Albaladejo, J.: Application of cluster analysis to
580 surface ozone, NO₂ and SO₂ daily patterns in an industrial area in Central-Southern
581 Spain measured with a DOAS system, *Sci. Total Environ.*, 429, 281-291, 2012.

582 AMAP/UNEP. Technical Background Report for the Global Mercury Assessment 2013.
583 UNEP Chemicals Branch Geneva, Switzerland. 2013.

584 Amyot, M., Mcqueen, D. J., Mierle, G., and Lean, D. R.: Sunlight-induced formation of
585 dissolved gaseous mercury in lake waters, *Environ. Sci. Technol.*, 28, 2366-2371,
586 1994.

587 Ashbaugh, L. L., Malm, W. C., and Sadeh, W. Z.: A residence time probability analysis of
588 sulfur concentrations at Grand Canyon National Park, *Atmospheric Environment*
589 (1967), 19, 1263-1270, 1985.

590 Begum, B. A., Kim, E., Biswas, S. K., and Hopke, P. K.: Investigation of sources of
591 atmospheric aerosol at urban and semi-urban areas in Bangladesh, *Atmos. Environ.*,
592 38, 3025-3038, 2004.

593 Brown, R. J., Goddard, S. L., Butterfield, D. M., Brown, A. S., Robins, C., Mustoe, C. L.,
594 and Mcghee, E. A.: Ten years of mercury measurement at urban and industrial air
595 quality monitoring stations in the UK, *Atmos. Environ.*, 109, 1-8, 2015.

596 Bullock, O. R., Brehme, K. A., and Mapp, G. R.: Lagrangian modeling of mercury air
597 emission, transport and deposition: an analysis of model sensitivity to emissions
598 uncertainty, *Sci. Total Environ.*, 213, 1-12, 1998.

599 Chen, L., Liu, M., Xu, Z., Fan, R., Tao, J., Chen, D., Zhang, D., Xie, D., and Sun, J.:
600 Variation trends and influencing factors of total gaseous mercury in the Pearl River
601 Delta—A highly industrialised region in South China influenced by seasonal
602 monsoons, *Atmos. Environ.*, 77, 757-766, 2013.

603 Cheng, I., Zhang, L., Mao, H., Blanchard, P., Tordon, R., and Dalziel, J.: Seasonal and
604 diurnal patterns of speciated atmospheric mercury at a coastal-rural and a coastal-
605 urban site, *Atmos. Environ.*, 82, 193-205, 2014.

606 Cheng, M. D., Hopke, P. K., and Zeng, Y.: A receptor-oriented methodology for determining
607 source regions of particulate sulfate observed at Dorset, Ontario, *Journal of
608 Geophysical Research: Atmospheres* (1984–2012), 98, 16839-16849, 1993.

609 Choi, E.-M., Kim, S.-H., Holsen, T. M., and Yi, S.-M.: Total gaseous concentrations in
610 mercury in Seoul, Korea: local sources compared to long-range transport from China
611 and Japan, *Environ. Pollut.*, 157, 816-822, 2009.

612 Choi, E., Heo, J.-B., Hopke, P. K., Jin, B.-B., and Yi, S.-M.: Identification, apportionment,
613 and photochemical reactivity of non-methane hydrocarbon sources in Busan, Korea,
614 *Water, Air, Soil Pollut.*, 215, 67-82, 2011.

615 Choi, H.-D., Huang, J., Mondal, S., and Holsen, T. M.: Variation in concentrations of three
616 mercury (Hg) forms at a rural and a suburban site in New York State, *Sci. Total
617 Environ.*, 448, 96-106, 2013.

618 Dommergue, A., Ferrari, C. P., Planchon, F. A., and Boutron, C. F.: Influence of
619 anthropogenic sources on total gaseous mercury variability in Grenoble suburban air
620 (France), *Sci. Total Environ.*, 297, 203-213, 2002.

621 Durnford, D., Dastoor, A., Figueras-Nieto, D., and Ryjkov, A.: Long range transport of
622 mercury to the Arctic and across Canada, *Atmospheric Chemistry and Physics*, 10,
623 6063-6086, 2010.

624 Dvonch, J., Graney, J., Marsik, F., Keeler, G., and Stevens, R.: An investigation of source-
 625 receptor relationships for mercury in south Florida using event precipitation data, *Sci. Total Environ.*, 213, 95-108, 1998.

626

627 Ebinghaus, R., Jennings, S., Kock, H., Derwent, R., Manning, A., and Spain, T.: Decreasing
 628 trends in total gaseous mercury observations in baseline air at Mace Head, Ireland
 629 from 1996 to 2009, *Atmos. Environ.*, 45, 3475-3480, 2011.

630 Fang, F., Wang, Q., and Li, J.: Urban environmental mercury in Changchun, a metropolitan
 631 city in Northeastern China: source, cycle, and fate, *Sci. Total Environ.*, 330, 159-170,
 632 2004.

633 Feng, X., Shang, L., Wang, S., Tang, S., and Zheng, W.: Temporal variation of total gaseous
 634 mercury in the air of Guiyang, China, *Journal of Geophysical Research: Atmospheres*
 635 (1984–2012), 109, 2004.

636 Flanders, J., Turner, R., Morrison, T., Jensen, R., Pizzuto, J., Skalak, K., and Stahl, R.:
 637 Distribution, behavior, and transport of inorganic and methylmercury in a high
 638 gradient stream, *Appl. Geochem.*, 25, 1756-1769, 2010.

639 Friedli, H., Arellano Jr, A., Geng, F., Cai, C., and Pan, L.: Measurements of atmospheric
 640 mercury in Shanghai during September 2009, *Atmos. Chem. Phys.*, 11, 3781-3788,
 641 2011.

642 Friedli, H. R., Radke, L. F., Prescott, R., Li, P., Woo, J. H., and Carmichael, G. R.: Mercury
 643 in the atmosphere around Japan, Korea, and China as observed during the 2001 ACE-
 644 Asia field campaign: Measurements, distributions, sources, and implications, *Journal*
 645 of *Geophysical Research: Atmospheres* (1984–2012), 109, 2004.

646 Fu, X., Feng, X., Dong, Z., Yin, R., Wang, J., Yang, Z., and Zhang, H.: Atmospheric gaseous
 647 elemental mercury (GEM) concentrations and mercury depositions at a high-altitude
 648 mountain peak in south China, *Atmos. Chem. Phys.*, 10, 2425-2437, 2010.

649 Fu, X., Feng, X., Zhu, W., Wang, S., and Lu, J.: Total gaseous mercury concentrations in
 650 ambient air in the eastern slope of Mt. Gongga, South-Eastern fringe of the Tibetan
 651 plateau, China, *Atmos. Environ.*, 42, 970-979, 2008.

652 Fu, X., Zhang, H., Lin, C.-J., Feng, X., Zhou, L., and Fang, S.: Correlation slopes of
 653 GEM/CO, GEM/CO 2, and GEM/CH 4 and estimated mercury emissions in China,
 654 South Asia, the Indochinese Peninsula, and Central Asia derived from observations in
 655 northwestern and southwestern China, *Atmos. Chem. Phys.*, 15, 1013-1028, 2015.

656 Gabriel, M. C., Williamson, D. G., Brooks, S., and Lindberg, S.: Atmospheric speciation of
 657 mercury in two contrasting Southeastern US airsheds, *Atmos. Environ.*, 39, 4947-
 658 4958, 2005.

659 Gauchard, P.-A., Ferrari, C. P., Dommergue, A., Poissant, L., Pilote, M., Guehenneux, G.,
 660 Boutron, C. F., and Baussand, P.: Atmospheric particle evolution during a nighttime
 661 atmospheric mercury depletion event in sub-Arctic at Kuujjuarapik/Whapmagoostui,
 662 Quebec, Canada, *Sci. Total Environ.*, 336, 215-224, 2005.

663 Gupta, A., Patil, R., and Gupta, S.: Emissions of gaseous and particulate pollutants in a port
 664 and harbour region in India, *Environ. Monit. Assess.*, 80, 187-205, 2002.

665 Hall, C. B., Mao, H., Ye, Z., Talbot, R., Ding, A., Zhang, Y., Zhu, J., Wang, T., Lin, C.-J.,
 666 and Fu, C.: Sources and Dynamic Processes Controlling Background and Peak
 667 Concentrations of TGM in Nanjing, China, *Atmosphere*, 5, 124-155, 2014.

668 Han, Y.-J., Holsen, T. M., Hopke, P. K., Cheong, J.-P., Kim, H., and Yi, S.-M.: Identification
 669 of source locations for atmospheric dry deposition of heavy metals during yellow-
 670 sand events in Seoul, Korea in 1998 using hybrid receptor models, *Atmos. Environ.*,
 671 38, 5353-5361, 2004.

672 Han, Y.-J., Holsen, T. M., Hopke, P. K., and Yi, S.-M.: Comparison between back-trajectory
 673 based modeling and Lagrangian backward dispersion modeling for locating sources of
 674 reactive gaseous mercury, *Environ. Sci. Technol.*, 39, 1715-1723, 2005.

675 Han, Y.-J., Kim, J.-E., Kim, P.-R., Kim, W.-J., Yi, S.-M., Seo, Y.-S., and Kim, S.-H.:
 676 General trends of atmospheric mercury concentrations in urban and rural areas in
 677 Korea and characteristics of high-concentration events, *Atmos. Environ.*, 94, 754-764,
 678 2014.

679 Heo, J.-B., Hopke, P., and Yi, S.-M.: Source apportionment of PM_{2.5} in Seoul, Korea, *Atmos.*
 680 *Chem. Phys.*, 9, 4957-4971, 2009.

681 Holmes, C. D., Jacob, D. J., Mason, R. P., and Jaffe, D. A.: Sources and deposition of
 682 reactive gaseous mercury in the marine atmosphere, *Atmos. Environ.*, 43, 2278-2285,
 683 2009.

684 Hopke, P., Barrie, L., Li, S. M., Cheng, M. D., Li, C., and Xie, Y.: Possible sources and
 685 preferred pathways for biogenic and non-sea-salt sulfur for the high Arctic, *Journal of*
 686 *Geophysical Research: Atmospheres* (1984–2012), 100, 16595-16603, 1995.

687 Hopke, P. K.: Recent developments in receptor modeling, *J. Chemometrics*, 17, 255-265,
 688 2003.

689 Hopke, P. K., Zhou, L., and Poirot, R. L.: Reconciling trajectory ensemble receptor model
 690 results with emissions, *Environ. Sci. Technol.*, 39, 7980-7983, 2005.

691 Hoyer, M., Burke, J., and Keeler, G. 1995. Atmospheric sources, transport and deposition of
 692 mercury in Michigan: two years of event precipitation. *Mercury as a Global*
 693 *Pollutant*. Springer.

694 Hsu, Y.-K., Holsen, T. M., and Hopke, P. K.: Comparison of hybrid receptor models to locate
 695 PCB sources in Chicago, *Atmos. Environ.*, 37, 545-562, 2003.

696 Huang, J., Choi, H.-D., Hopke, P. K., and Holsen, T. M.: Ambient mercury sources in
 697 Rochester, NY: results from principle components analysis (PCA) of mercury
 698 monitoring network data, *Environ. Sci. Technol.*, 44, 8441-8445, 2010.

699 Jaffe, D., Prestbo, E., Swartzendruber, P., Weiss-Penzias, P., Kato, S., Takami, A.,
 700 Hatakeyama, S., and Kajii, Y.: Export of atmospheric mercury from Asia, *Atmos.*
 701 *Environ.*, 39, 3029-3038, 2005.

702 Jen, Y.-H., Yuan, C.-S., Hung, C.-H., Ie, I.-R., and Tsai, C.-M.: Tempospatial variation and
 703 partition of atmospheric mercury during wet and dry seasons at sensitivity sites within
 704 a heavily polluted industrial city, *Aerosol Air Qual. Res.*, 13, 13-23, 2013.

705 Keeler, G., and Barres, J.: Sampling and Analysis for Atmospheric Mercury, Center for
 706 Environmental Research Information, Cincinnati, 1999.

707 Kellerhals, M., Beauchamp, S., Belzer, W., Blanchard, P., Froude, F., Harvey, B., McDonald,
 708 K., Pilote, M., Poissant, L., and Puckett, K.: Temporal and spatial variability of total
 709 gaseous mercury in Canada: results from the Canadian Atmospheric Mercury
 710 Measurement Network (CAMNet), *Atmos. Environ.*, 37, 1003-1011, 2003.

711 Kim, E., Hopke, P. K., and Edgerton, E. S.: Source identification of Atlanta aerosol by
 712 positive matrix factorization, *J. Air Waste Manage. Assoc.*, 53, 731-739, 2003a.

713 Kim, E., Larson, T. V., Hopke, P. K., Slaughter, C., Sheppard, L. E., and Claiborn, C.: Source
 714 identification of PM_{2.5} in an arid Northwest US City by positive matrix factorization,
 715 *Atmospheric Research*, 66, 291-305, 2003b.

716 Kim, J.-H., Park, J.-M., Lee, S.-B., Pudasainee, D., and Seo, Y.-C.: Anthropogenic mercury
 717 emission inventory with emission factors and total emission in Korea, *Atmos.*
 718 *Environ.*, 44, 2714-2721, 2010.

719 Kim, K.-H., Brown, R. J., Kwon, E., Kim, I.-S., and Sohn, J.-R.: Atmospheric mercury at an
 720 urban station in Korea across three decades, *Atmos. Environ.*, 131, 124-132, 2016.

721 Kim, K.-H., and Kim, M.-Y.: The effects of anthropogenic sources on temporal distribution
 722 characteristics of total gaseous mercury in Korea, *Atmos. Environ.*, 34, 3337-3347,
 723 2000.

724 Kim, K.-H., and Kim, M.-Y.: Some insights into short-term variability of total gaseous
 725 mercury in urban air, *Atmos. Environ.*, 35, 49-59, 2001.

726 Kim, S.-H., Han, Y.-J., Holsen, T. M., and Yi, S.-M.: Characteristics of atmospheric
 727 speciated mercury concentrations (TGM, Hg (II) and Hg (p)) in Seoul, Korea, *Atmos.*
 728 *Environ.*, 43, 3267-3274, 2009.

729 Kuo, T.-H., Chang, C.-F., Urba, A., and Kvietkus, K.: Atmospheric gaseous mercury in
 730 Northern Taiwan, *Sci. Total Environ.*, 368, 10-18, 2006.

731 Lai, S.-O., Holsen, T. M., Hopke, P. K., and Liu, P.: Wet deposition of mercury at a New
 732 York state rural site: concentrations, fluxes, and source areas, *Atmos. Environ.*, 41,
 733 4337-4348, 2007.

734 Laurier, F. J., Mason, R. P., Whalin, L., and Kato, S.: Reactive gaseous mercury formation in
 735 the North Pacific Ocean's marine boundary layer: A potential role of halogen
 736 chemistry, *Journal of Geophysical Research: Atmospheres* (1984–2012), 108, 2003.

737 Lee, D. S., Dollard, G. J., and Pepler, S.: Gas-phase mercury in the atmosphere of the United
 738 Kingdom, *Atmos. Environ.*, 32, 855-864, 1998.

739 Lee, S. J., Seo, Y.-C., Jurng, J., Hong, J.-H., Park, J.-W., Hyun, J. E., and Lee, T. G.:
 740 Mercury emissions from selected stationary combustion sources in Korea, *Sci. Total*
 741 *Environ.*, 325, 155-161, 2004.

742 Li, Z., Xia, C., Wang, X., Xiang, Y., and Xie, Z.: Total gaseous mercury in Pearl River Delta
 743 region, China during 2008 winter period, *Atmos. Environ.*, 45, 834-838, 2011.

744 Lim, C.-J., Cheng, M.-D., and Schroeder, W. H.: Transport patterns and potential sources of
 745 total gaseous mercury measured in Canadian high Arctic in 1995, *Atmos. Environ.*,
 746 35, 1141-1154, 2001.

747 Lin, C.-J., and Pehkonen, S. O.: The chemistry of atmospheric mercury: a review, *Atmos.*
 748 *Environ.*, 33, 2067-2079, 1999.

749 Lin, C.-J., Pongprueksa, P., Lindberg, S. E., Pehkonen, S. O., Byun, D., and Jang, C.:
 750 Scientific uncertainties in atmospheric mercury models I: Model science evaluation,
 751 *Atmos. Environ.*, 40, 2911-2928, 2006.

752 Lindberg, S., Bullock, R., Ebinghaus, R., Engstrom, D., Feng, X., Fitzgerald, W., Pirrone, N.,
 753 Prestbo, E., and Seigneur, C.: A synthesis of progress and uncertainties in attributing
 754 the sources of mercury in deposition, *AMBIO: A Journal of the Human Environment*,
 755 36, 19-33, 2007.

756 Liu, N., Qiu, G., Landis, M. S., Feng, X., Fu, X., and Shang, L.: Atmospheric mercury
 757 species measured in Guiyang, Guizhou province, southwest China, *Atmospheric*
 758 *Research*, 100, 93-102, 2011.

759 Lu, J. Y., and Schroeder, W. H.: Annual time-series of total filterable atmospheric mercury
 760 concentrations in the Arctic, *Tellus B*, 56, 213-222, 2004.

761 Lynam, M. M., and Keeler, G. J.: Source–receptor relationships for atmospheric mercury in
 762 urban Detroit, Michigan, *Atmos. Environ.*, 40, 3144-3155, 2006.

763 Mao, H., Talbot, R., Sigler, J., Sive, B., and Hegarty, J.: Seasonal and diurnal variations of
 764 Hg over New England, *Atmos. Chem. Phys.*, 8, 1403-1421, 2008.

765 Marumoto, K., Hayashi, M., and Takami, A.: Atmospheric mercury concentrations at two
 766 sites in the Kyushu Islands, Japan, and evidence of long-range transport from East
 767 Asia, *Atmos. Environ.*, 117, 147-155, 2015.

768 Mason, R. P., and Sheu, G. R.: Role of the ocean in the global mercury cycle, *Global*
 769 *biogeochemical cycles*, 16, 40-1-40-14, 2002.

770 Miller, C. L., Watson, D. B., Lester, B. P., Lowe, K. A., Pierce, E. M., and Liang, L.:
 771 Characterization of soils from an industrial complex contaminated with elemental
 772 mercury, *Environ. Res.*, 125, 20-29, 2013.

773 Muntean, M., Janssens-Maenhout, G., Song, S., Selin, N. E., Olivier, J. G., Guizzardi, D.,
 774 Maas, R., and Dentener, F.: Trend analysis from 1970 to 2008 and model evaluation
 775 of EDGARv4 global gridded anthropogenic mercury emissions, *Sci. Total Environ.*,
 776 494, 337-350, 2014.

777 Nakagawa, R.: Studies on the levels in atmospheric concentrations of mercury in Japan,
 778 *Chemosphere*, 31, 2669-2676, 1995.

779 Nier: National Air Pollutants Emission 2011 (in Korean), 2011.

780 Obrist, D., Tas, E., Peleg, M., Matveev, V., Faïn, X., Asaf, D., and Luria, M.: Bromine-
 781 induced oxidation of mercury in the mid-latitude atmosphere, *Nature Geoscience*, 4,
 782 22-26, 2011.

783 Osawa, T., Ueno, T., and Fu, F.: Sequential variation of atmospheric mercury in Tokai-mura,
 784 seaside area of eastern central Japan, *Journal of Geophysical Research: Atmospheres*
 785 (1984–2012), 112, 2007.

786 Pacyna, E. G., Pacyna, J., Sundseth, K., Munthe, J., Kindbom, K., Wilson, S., Steenhuisen,
 787 F., and Maxson, P.: Global emission of mercury to the atmosphere from
 788 anthropogenic sources in 2005 and projections to 2020, *Atmos. Environ.*, 44, 2487-
 789 2499, 2010.

790 Pacyna, E. G., Pacyna, J. M., Steenhuisen, F., and Wilson, S.: Global anthropogenic mercury
 791 emission inventory for 2000, *Atmos. Environ.*, 40, 4048-4063, 2006.

792 Pacyna, J. M., Pacyna, E. G., Steenhuisen, F., and Wilson, S.: Mapping 1995 global
 793 anthropogenic emissions of mercury, *Atmos. Environ.*, 37, 109-117, 2003.

794 Pirrone, N., Aas, W., Cinnirella, S., Ebinghaus, R., Hedgecock, I. M., Pacyna, J., Sprovieri,
 795 F., and Sunderland, E. M.: Toward the next generation of air quality monitoring:
 796 Mercury, *Atmos. Environ.*, 80, 599-611, 2013.

797 Pirrone, N., Cinnirella, S., Feng, X., Finkelman, R., Friedli, H., Leaner, J., Mason, R.,
 798 Mukherjee, A., Stracher, G., and Streets, D.: Global mercury emissions to the
 799 atmosphere from anthropogenic and natural sources, *Atmospheric Chemistry and
 800 Physics*, 10, 5951-5964, 2010.

801 Poissant, L.: Potential sources of atmospheric total gaseous mercury in the St. Lawrence
 802 River valley, *Atmos. Environ.*, 33, 2537-2547, 1999.

803 Polissar, A. V., Hopke, P. K., and Harris, J. M.: Source regions for atmospheric aerosol
 804 measured at Barrow, Alaska, *Environ. Sci. Technol.*, 35, 4214-4226, 2001.

805 Sakata, M., and Marumoto, K.: Formation of atmospheric particulate mercury in the Tokyo
 806 metropolitan area, *Atmos. Environ.*, 36, 239-246, 2002.

807 Sakata, M., and Marumoto, K.: Wet and dry deposition fluxes of mercury in Japan, *Atmos.*
 808 *Environ.*, 39, 3139-3146, 2005.

809 Schmolke, S. R., Schroeder, W., Kock, H., Schneeberger, D., Munthe, J., and Ebinghaus, R.:
 810 Simultaneous measurements of total gaseous mercury at four sites on a 800km
 811 transect: spatial distribution and short-time variability of total gaseous mercury over
 812 central Europe, *Atmos. Environ.*, 33, 1725-1733, 1999.

813 Schroeder, W. H., and Munthe, J.: Atmospheric mercury—an overview, *Atmos. Environ.*, 32,
 814 809-822, 1998.

815 Seo, Y.-S., Han, Y.-J., Choi, H.-D., Holsen, T. M., and Yi, S.-M.: Characteristics of total
 816 mercury (TM) wet deposition: scavenging of atmospheric mercury species, *Atmos.*
 817 *Environ.*, 49, 69-76, 2012.

818 Seo, Y.-S., Han, Y.-J., Holsen, T. M., Choi, E., Zoh, K.-D., and Yi, S.-M.: Source
 819 identification of total mercury (TM) wet deposition using a Lagrangian particle
 820 dispersion model (LPDM), *Atmos. Environ.*, 104, 102-111, 2015.

821 Shon, Z.-H., Kim, K.-H., Kim, M.-Y., and Lee, M.: Modeling study of reactive gaseous
 822 mercury in the urban air, *Atmos. Environ.*, 39, 749-761, 2005.

823 Slemr, F., Brunke, E. G., Ebinghaus, R., Temme, C., Munthe, J., Wängberg, I., Schroeder,
 824 W., Steffen, A., and Berg, T.: Worldwide trend of atmospheric mercury since 1977,
 825 *Geophys. Res. Lett.*, 30, 2003.

826 Song, X., Cheng, I., and Lu, J.: Annual atmospheric mercury species in downtown Toronto,
 827 Canada, *J. Environ. Monit.*, 11, 660-669, 2009.

828 Sprovieri, F., Pirrone, N., Ebinghaus, R., Kock, H., and Dommergues, A.: A review of
 829 worldwide atmospheric mercury measurements, *Atmos. Chem. Phys.*, 10, 8245-8265,
 830 2010.

831 Stamenkovic, J., Lyman, S., and Gustin, M. S.: Seasonal and diel variation of atmospheric
 832 mercury concentrations in the Reno (Nevada, USA) airshed, *Atmos. Environ.*, 41,
 833 6662-6672, 2007.

834 Stohl, A., Eckhardt, S., Forster, C., James, P., Spichtinger, N., and Seibert, P.: A replacement
 835 for simple back trajectory calculations in the interpretation of atmospheric trace
 836 substance measurements, *Atmos. Environ.*, 36, 4635-4648, 2002.

837 Streets, D. G., Devane, M. K., Lu, Z., Bond, T. C., Sunderland, E. M., and Jacob, D. J.: All-
 838 time releases of mercury to the atmosphere from human activities, *Environ. Sci.
 839 Technol.*, 45, 10485-10491, 2011.

840 Strode, S. A., Jaeglé, L., Selin, N. E., Jacob, D. J., Park, R. J., Yantosca, R. M., Mason, R. P.,
 841 and Slemr, F.: Air-sea exchange in the global mercury cycle, *Global Biogeochemical
 842 Cycles*, 21, 2007.

843 Temme, C., Blanchard, P., Steffen, A., Banic, C., Beauchamp, S., Poissant, L., Tordon, R.,
 844 and Wiens, B.: Trend, seasonal and multivariate analysis study of total gaseous
 845 mercury data from the Canadian atmospheric mercury measurement network
 846 (CAMNet), *Atmos. Environ.*, 41, 5423-5441, 2007.

847 UNEP: *Global mercury assessment*. UNEP Chemicals, 2002.

848 UNEP: The global atmospheric mercury assessment: Sources, emissions and transport,
 849 [http://www.unep.org/chemicalsandwaste/Portals/9/Mercury/Documents/Publications/
 850 UNEP_GlobalAtmosphericMercuryAssessment_May2009.pdf](http://www.unep.org/chemicalsandwaste/Portals/9/Mercury/Documents/Publications/UNEP_GlobalAtmosphericMercuryAssessment_May2009.pdf), 2008.

851 Uria-Tellaetxe, I., and Carslaw, D. C.: Conditional bivariate probability function for source
 852 identification, *Environ. Model. Software*, 59, 1-9, 2014.

853 Wan, Q., Feng, X., Lu, J., Zheng, W., Song, X., Han, S., and Xu, H.: Atmospheric mercury in
 854 Changbai Mountain area, northeastern China I. The seasonal distribution pattern of
 855 total gaseous mercury and its potential sources, *Environ. Res.*, 109, 201-206, 2009.

856 Weigelt, A., Ebinghaus, R., Manning, A., Derwent, R., Simmonds, P., Spain, T., Jennings, S.,
 857 and Slemr, F.: Analysis and interpretation of 18 years of mercury observations since
 858 1996 at Mace Head, Ireland, *Atmos. Environ.*, 100, 85-93, 2015.

859 Weiss-Penzias, P., Jaffe, D., Swartzendruber, P., Hafner, W., Chand, D., and Prestbo, E.:
 860 Quantifying Asian and biomass burning sources of mercury using the Hg/CO ratio in
 861 pollution plumes observed at the Mount Bachelor Observatory, *Atmos. Environ.*, 41,
 862 4366-4379, 2007.

863 Weiss-Penzias, P., Jaffe, D. A., Mcclintick, A., Prestbo, E. M., and Landis, M. S.: Gaseous
 864 elemental mercury in the marine boundary layer: Evidence for rapid removal in
 865 anthropogenic pollution, *Environ. Sci. Technol.*, 37, 3755-3763, 2003.

866 Weiss-Penzias, P., Jaffe, D. A., Swartzendruber, P., Dennison, J. B., Chand, D., Hafner, W.,
867 and Prestbo, E.: Observations of Asian air pollution in the free troposphere at Mount
868 Bachelor Observatory during the spring of 2004, *Journal of Geophysical Research: Atmospheres* (1984–2012), 111, 2006.

870 Wilson, S., Munthe, J., Sundseth, K., Maxson, P., Kindbom, K., Pacyna, J., and Steenhuisen,
871 F. Updating Historical Global Inventories of Anthropogenic Mercury Emissions to
872 Air. *AMAP Technical Report No. 3* (2010). Arctic Monitoring and Assessment
873 Programme (AMAP). 2010.

874 Xie, Y., and Berkowitz, C. M.: The use of positive matrix factorization with conditional
875 probability functions in air quality studies: an application to hydrocarbon emissions in
876 Houston, Texas, *Atmos. Environ.*, 40, 3070-3091, 2006.

877 Zeng, Y., and Hopke, P.: A study of the sources of acid precipitation in Ontario, Canada,
878 *Atmospheric Environment* (1967), 23, 1499-1509, 1989.

879 Zhang, H., and Lindberg, S. E.: Sunlight and iron (III)-induced photochemical production of
880 dissolved gaseous mercury in freshwater, *Environ. Sci. Technol.*, 35, 928-935, 2001.

881 Zhang, L., Wang, S., Wang, L., Wu, Y., Duan, L., Wu, Q., Wang, F., Yang, M., Yang, H.,
882 Hao, J., and Liu, X.: Updated emission inventories for speciated atmospheric mercury
883 from anthropogenic sources in China, *Environ. Sci. Technol.*, 49, 3185-94, 2015.

884 Zhao, W., Hopke, P. K., and Karl, T.: Source identification of volatile organic compounds in
885 Houston, Texas, *Environ. Sci. Technol.*, 38, 1338-1347, 2004.

886 Zhou, L., Kim, E., Hopke, P. K., Stanier, C. O., and Pandis, S.: Advanced factor analysis on
887 Pittsburgh particle size-distribution data special issue of aerosol science and
888 technology on findings from the Fine Particulate Matter Supersites Program, *Aerosol
889 Science and Technology*, 38, 118-132, 2004.